Published May 30, 2011

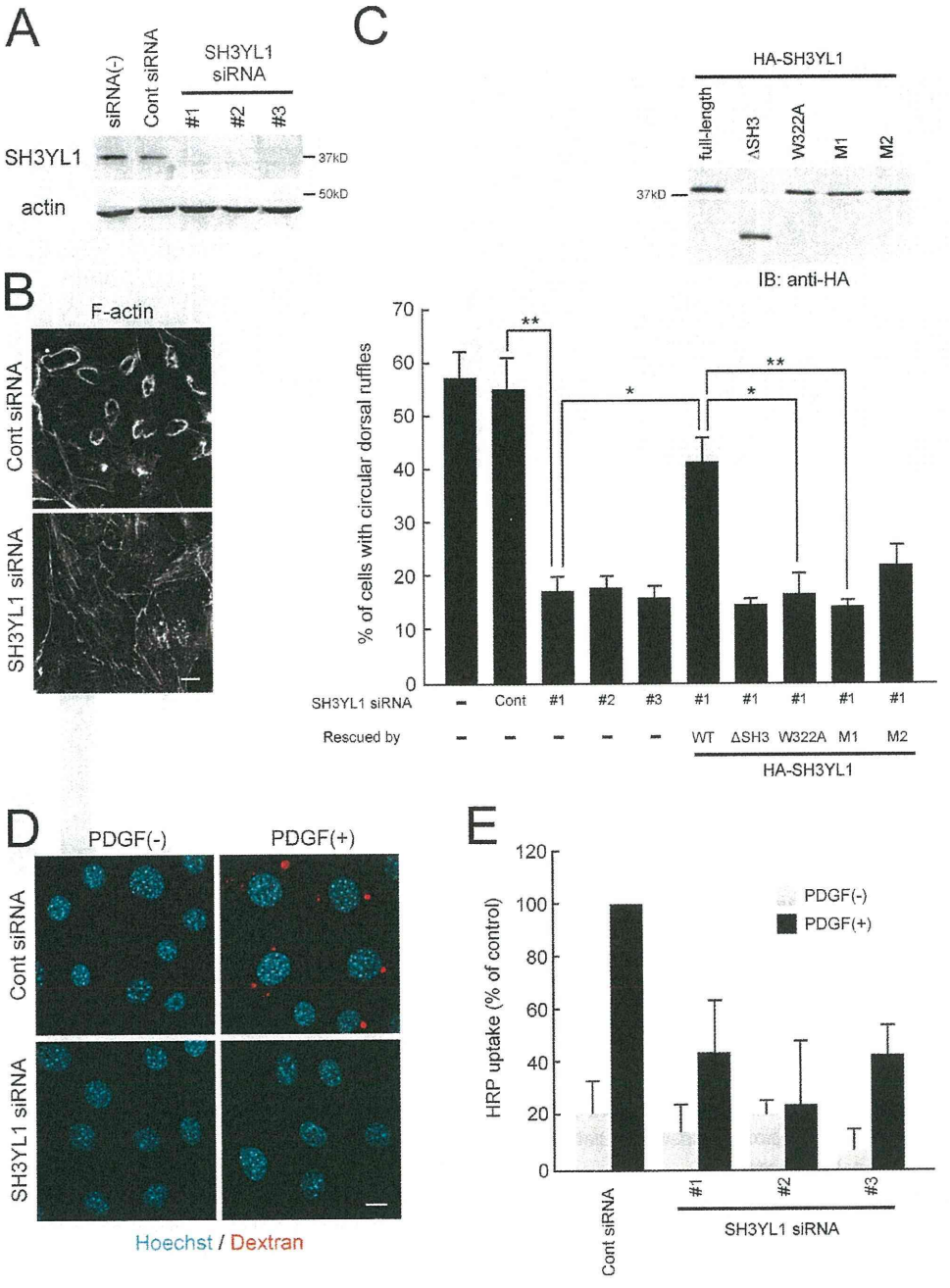

Figure 4. **SH3YL1 is necessary for dorsal ruffle formation.** (A) Anti-SH3YL1 immunoblots of NIH3T3 cells transfected with control or SH3YL1-specific siRNA. (B) Phalloidin staining of control or SH3YL1-depleted NIH3T3 cells treated with PDGF for 5 min. Bar, 10 µm. (C) Percentages of cells generating at least one circular dorsal ruffle. Rescue experiments were performed by transfecting HA-SH3YL1 constructs (blot, expression levels of the indicated constructs) to recover circular dorsal ruffle formation. Results are a mean (SD) of three independent experiments; 200 cells counted (100 cells for the rescue experiments) per experiment. **, $P < 0.01$; *, $P < 0.05$. (D) Control or SH3YL1-depleted NIH3T3 cells were allowed to internalize the fluid-phase marker rhodamine-dextran (0.2 mg/ml; shown in red) for 10 min and then stained with Hoechst (cyan). Bar, 10 µm. (E) NIH3T3 cells transfected with indicated siRNAs were subjected to HRP uptake assay for 10 min with or without PDGF stimulation (20 ng/ml). Results are a mean (SD) of three independent experiments.

marker of fluid-phase endocytosis. Knockdown of SH3YL1 expression by all three siRNAs resulted in a significant reduction in the PDGF-induced internalization of HRP (Fig. 4 E). These data demonstrate that the SH3YL1–phosphoinositide interaction regulates PDGF-induced dorsal ruffle formation and macropinocytosis.

SH3YL1 forms a complex with SHIP2, a phosphoinositide 5-phosphatase

To determine the molecular mechanism by which SH3YL1 mediates dorsal ruffle formation, we attempted to identify its binding proteins. The SH3 domain of SH3YL1 was expressed as a GST fusion protein and was used in a pull-down assay with

Published May 30, 2011

HeLa cell lysates. Several proteins were identified, including N-WASP and dynamin 2, which are typical binding partners for SH3 domains (Fig. 5 A).

Notably, SHIP2, a PI(3,4,5)P_3 5-phosphatase that generates PI(3,4)P_2, was also identified in the pull-down fraction (Fig. 5 A). We decided to focus on this interaction because of its potential relevance to SH3YL1 function in PI3K-dependent dorsal ruffle formation. This interaction was reproduced using exogenous Myc-tagged SHIP2 (Myc-SHIP2), which was pulled down by GST-SH3 and GST-SH3YL1 (full length) but not by GST (Fig. 5 B). Moreover, SH3YL1 and SHIP2 interacted with each other in the HeLa cells that were transfected with FLAG-tagged SH3YL1 (FLAG-SH3YL1). As shown in Fig. 5 C, endogenous SHIP2 was detected in anti-FLAG immunoprecipitates from the lysates of FLAG-SH3YL1 (full length)–transfected cells but not from lysates of cells that were transfected with ΔSH3 or W322A, wherein a highly conserved tryptophan residue in the SH3 domain was mutated; this suggested that SH3YL1 interacts with SHIP2 through its SH3 domain. The W322A mutant was unable to rescue the impaired dorsal ruffle formation in SH3YL1 knockdown NIH3T3 cells (Fig. 4 C). Endogenous SHIP2 was detected in the anti-SH3YL1 immunoprecipitates from NIH3T3 cell lysates, further indicating that they form a complex in vivo (Fig. 5 D). We also determined this interaction to be direct, as shown in pull-down experiments using purified FLAG-SHIP2 (Fig. 5 E).

The C-terminal region of SHIP2 is rich in proline residues and mediates several interactions with SH3 domain–containing proteins (Fig. 5 F; Dyson et al., 2001; Xie et al., 2008). To our surprise, the deletion of a C-terminal region, including the proline-rich area (SHIP2 (1–740)), did not alter the coimmunoprecipitation of SHIP2 with SH3YL1 (Fig. 5 G). Conversely, deletion of the SH2 domain and a flanking region that is on the N-terminal side of the lipid phosphatase domain (SHIP2 (415–1,258)) nearly abolished the binding. In this flanking region, we identified an amino acid sequence, PPLPPR, that matched the class II consensus motif of SH3 domain–binding peptide (Mayer and Gupta, 1998; Kang et al., 2000). Indeed, the deletion (SHIP2 (Δ139–144)) and mutation (SHIP2 (PL140,141AA)) of this sequence resulted in loss of binding (Fig. 5 G).

We also examined whether the interaction between SH3YL1 and SHIP2 was regulated by growth factor stimulation. FLAG-SH3YL1–expressing NIH3T3 cells were treated with PDGF followed by immunoprecipitation with anti-FLAG. Compared with serum-starved conditions (0 min), the interaction significantly increased 5 min after PDGF treatment (Fig. 5 H). These results demonstrate that SH3YL1 and SHIP2 form a molecular complex through an interaction between the N-terminal proline-rich sequence in SHIP2 and the C-terminal SH3 domain of SH3YL1 that is regulated by PDGF.

SHIP2 is required for circular dorsal ruffle formation

To determine the function of SHIP2 in dorsal ruffle formation, NIH3T3 cells were transfected with Myc-SHIP2 and HA-SH3YL1 and stimulated with PDGF. As a result, significant colocalization of SH3YL1 and SHIP2 was observed at the circular dorsal ruffles (Fig. 6 A).

The function of SHIP2 was further examined in knockdown experiments (Fig. 6 B). In SHIP2 knockdown cells, the formation of ring-shaped circular dorsal ruffles was impaired, whereas the ruffles in the peripheral membrane remained intact (Fig. 6, C [arrow] and D). Notably, several relatively straight ruffles were formed at the dorsal plasma membrane, to which SH3YL1 also localized (Fig. 6, C [arrowheads], D, and E [arrows]). These effects were specifically suppressed by exogenous SHIP2, depending on its interaction with SH3YL1 (Fig. 6 D). The straight ruffles that were induced by SHIP2 knockdown are possibly malformed dorsal ruffles that cannot develop ring-shaped structures. Correspondingly, dextran uptake was also inhibited in SHIP2-depleted cells (Fig. 6 F). These data imply that SHIP2 functions with SH3YL1 and that SHIP2 mediates the formation of the circular membrane structure.

As shown in Fig. 5 A, our pull-down experiment also identified PI3K-C2β as a binding partner for the SH3 domain of SH3YL1. We confirmed this interaction of FLAG-SH3YL1 and endogenous PI3K-C2β (Fig. S3 A). Myc-tagged PI3K-C2β localized to the dorsal ruffles, and its suppression, as mediated by expression knockdown, inhibited dorsal ruffle formation (Fig. S3, B [top row], C, and E), indicating its importance.

SH3YL1 and SHIP2 are required for the production of PI(3,4)P_2, whose downstream target is necessary for circular dorsal ruffle formation

The preferred substrate for SHIP2 is PI(3,4,5)P_3, which generates PI(3,4)P_2 (Ishihara et al., 1999). To investigate the relationship between PI(3,4)P_2 levels and dorsal ruffle formation, we measured cellular levels of phosphoinositides after stimulation with PDGF by dot-blot assay. Production of PI(3,4,5)P_3 increased 2 min after stimulation with PDGF, when the dorsal ruffles were scarce (Fig. 7, A and B; and Fig. S5 A). In contrast, the generation of PI(3,4)P_2 was delayed compared with PI(3,4,5)P_3 and peaked 5 min after stimulation, when the formation of circular dorsal ruffles was nearly complete (Fig. 7, A and B). This result implies a link between PI(3,4)P_2 production and circular dorsal ruffle formation.

PI(3,4)P_2 production was significantly inhibited in SH3YL1- or SHIP2 siRNA–treated cells (Figs. 7 A [middle] and S5 A). In SH3YL1 knockdown cells, PI(3,4,5)P_3 synthesis was also reduced (Figs. 7 A [top] and S5 A). Considering the involvement of SH3YL1 and SHIP2 in dorsal ruffle formation (Figs. 4, B and C; and 6, C and D), these results strongly suggest that PI(3,4)P_2 is a prerequisite for this process.

Consistent with a previous study (Hogan et al., 2004), overexpression of Tapp1 pleckstrin homology (PH) domain, which possibly blocks endogenous PI(3,4)P_2-binding proteins in a competitive manner, suppressed dorsal ruffle formation (Fig. 7 C). Knockdown of endogenous Tapp1 also suppressed dorsal ruffle formation (Fig. S3, D and E), suggesting that Tapp1 is a downstream target of PI(3,4)P_2, which is required in this process. In support of this model, we observed that the exogenous HA-Tapp1 localized to the circular dorsal ruffles (Fig. S3 B, bottom row).

Overexpression of Grp1PH also inhibited dorsal ruffle formation (Fig. 7 C), implying that PI(3,4,5)P_3 is necessary.

Published May 30, 2011

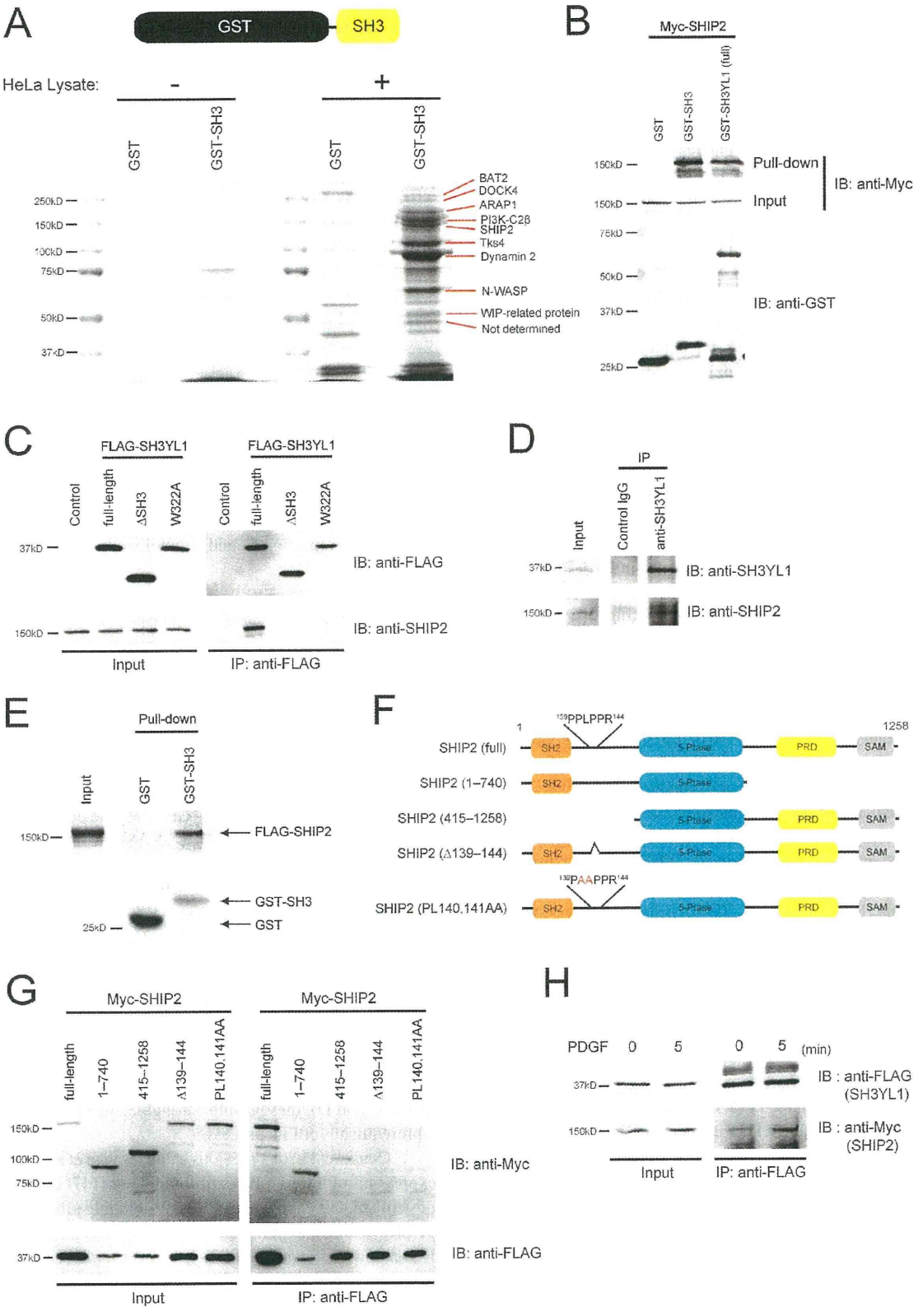

Figure 5. **SH3YL1 forms a complex with SHIP2.** (A) The GST or GST-SH3 domain of SH3YL1 was incubated with (+) or without (−) HeLa cell lysates. Bound fractions were visualized by CBB staining. Proteins identified by mass spectrometry are shown. (B) Lysates of COS-1 cells expressing Myc-SHIP2 were pulled down by GST, GST fusions with the SH3 domain, or full-length SH3YL1 and then immunoblotted with anti-Myc or anti-GST antibodies. (C) FLAG-SH3YL1 (full

Published May 30, 2011

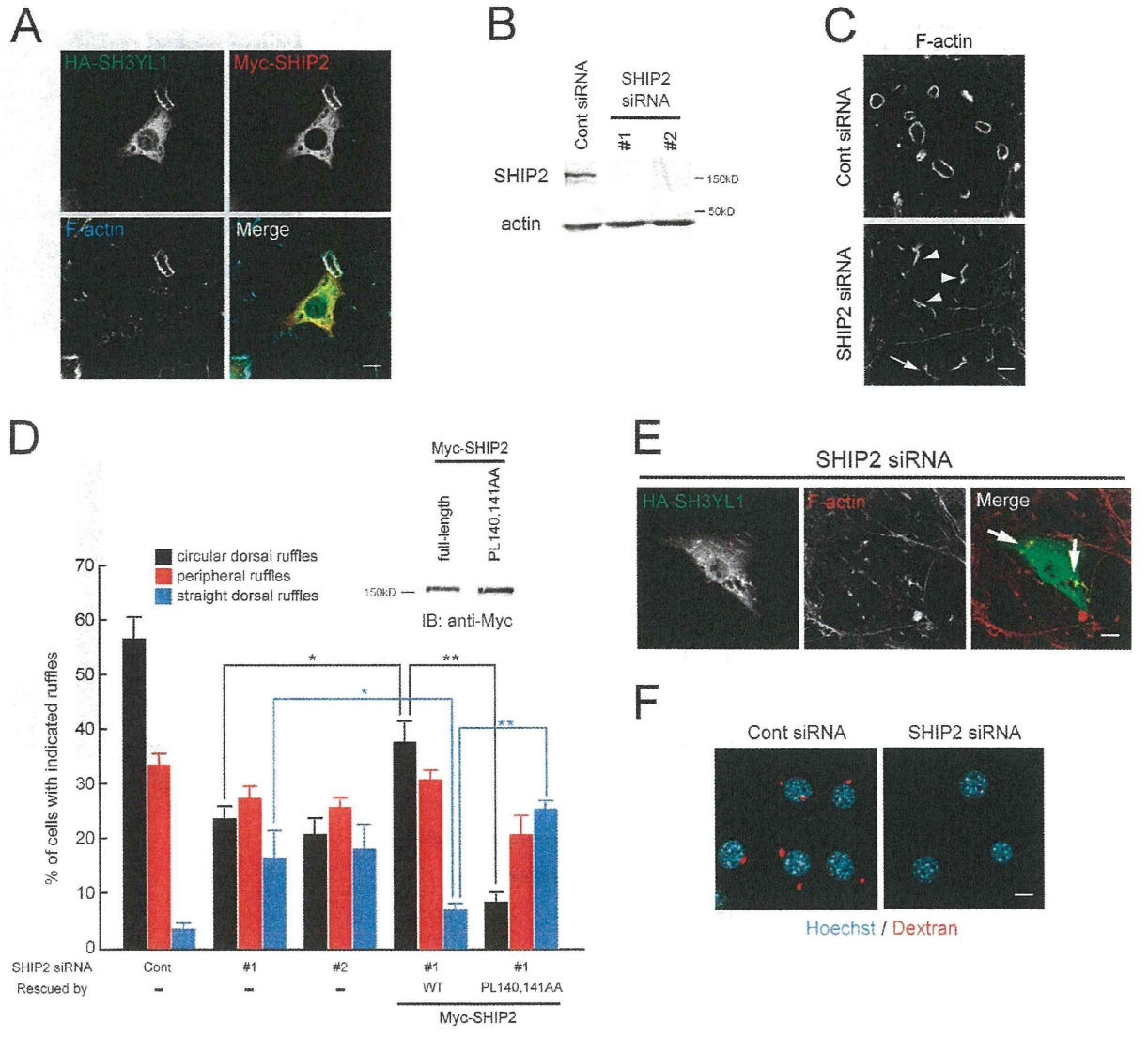

Figure 6. **SHIP2 is required for circular dorsal ruffle formation.** (A) NIH3T3 cells transiently transfected with HA-SH3YL1 and Myc-SHIP2 were serum starved, stimulated with 20 ng/ml PDGF for 5 min, fixed, and stained with anti-HA, anti-Myc antibodies, and Alexa Fluor 647–phalloidin. Bar, 10 µm. (B) Anti-SHIP2 immunoblots of NIH3T3 cells transfected with control or SHIP2-specific siRNA. (C) PDGF-induced circular dorsal ruffle formation was reduced in SHIP2-depleted NIH3T3 cells. Phalloidin staining of cells treated with control or SHIP2 siRNAs is shown. The arrow indicates peripheral ruffles, and arrowheads indicate straight dorsal ruffles. Bar, 10 µm. (D) Percentages of cells generating at least one circular dorsal ruffle, peripheral ruffle, or straight dorsal ruffle. Rescue experiments were performed by transfecting Myc-SHIP2 constructs (blot, expression levels of the indicated constructs) to recover each ruffle formation. WT, wild type. Results are a mean (SD) of three independent experiments; 200 cells counted (100 cells for the rescue experiments) per experiment. **, $P < 0.01$ and *, $P < 0.05$. (E) SHIP2-depleted NIH3T3 cells transiently transfected with HA-SH3YL1 were serum starved, stimulated with 20 ng/ml PDGF for 5 min, fixed, and stained with anti-HA antibodies and rhodamine-phalloidin. Arrows indicate straight dorsal ruffles. Bar, 10 µm. (F) Rhodamine-dextran (red) and Hoechst (cyan) images of NIH3T3 cells treated with SHIP2 or control siRNA and incubated for 10 min with 0.2 mg/ml rhodamine-dextran. Bar, 10 µm.

length, ΔSH3, or W322A) expressed in HeLa cells was immunoprecipitated with anti-FLAG antibodies and immunoblotted with anti-FLAG or anti-SHIP2 antibodies. (D) Endogenous SH3YL1 was immunoprecipitated with anti-SH3YL1 antibodies using lysates of NIH3T3 cells and immunoblotted with anti-SH3YL1 or anti-SHIP2 antibodies. (E) Purified FLAG-SHIP2 was pulled down by GST and GST fusions with the SH3 domain and then visualized by CBB staining. (F) A schematic presentation of SHIP2 deletion and point mutants used in this study. The red text indicates introduced alanines instead of intact amino acids (proline and leucine). PRD, proline-rich domain; SAM, sterile α motif. (G) FLAG-SH3YL1 (full length) and the indicated Myc-SHIP2 mutants expressed in COS-1 cells were immunoprecipitated with anti-FLAG antibodies and immunoblotted with anti-FLAG or anti-Myc antibodies. (H) NIH3T3 cells transiently transfected with FLAG-SH3YL1 and Myc-SHIP2 were serum starved and then stimulated with 20 ng/ml PDGF for 0 and 5 min. Cells were harvested, and the lysate was immunoprecipitated with anti-FLAG antibodies and immunoblotted with anti-FLAG or anti-Myc antibodies.

Published May 30, 2011

Figure 7. **Correlation between PI(3,4)P_2 synthesis and circular dorsal ruffle formation.** (A) Lipids were extracted from control, SH3YL1-, or SHIP2-depleted NIH3T3 stimulated with 20 ng/ml PDGF for 0, 2, 5, and 15 min. Amounts of PI(3,4)P_2, PI(4,5)P_2, and PI(3,4,5)P_3 were quantified by Qdot-705-Tapp1-2xPH, Qdot-655-PLCδ1-PH, and Qdot-585-Grp1-PH, respectively, in the dot-blot assay. Data are a mean (SD) of three independent experiments. (B) Time course of circular dorsal ruffle formation. Phalloidin staining and quantifications are shown. Results are a mean (SD) of three independent experiments; 200 cells counted per experiment. Bar, 10 µm. (C) Quantification of circular dorsal ruffles in NIH3T3 cells overexpressing lipid-binding domains. Percentages of cells with at least one circular dorsal ruffle are shown. Results are a mean (SD) of three independent experiments; 100 cells counted per experiment. **, $P < 0.01$.

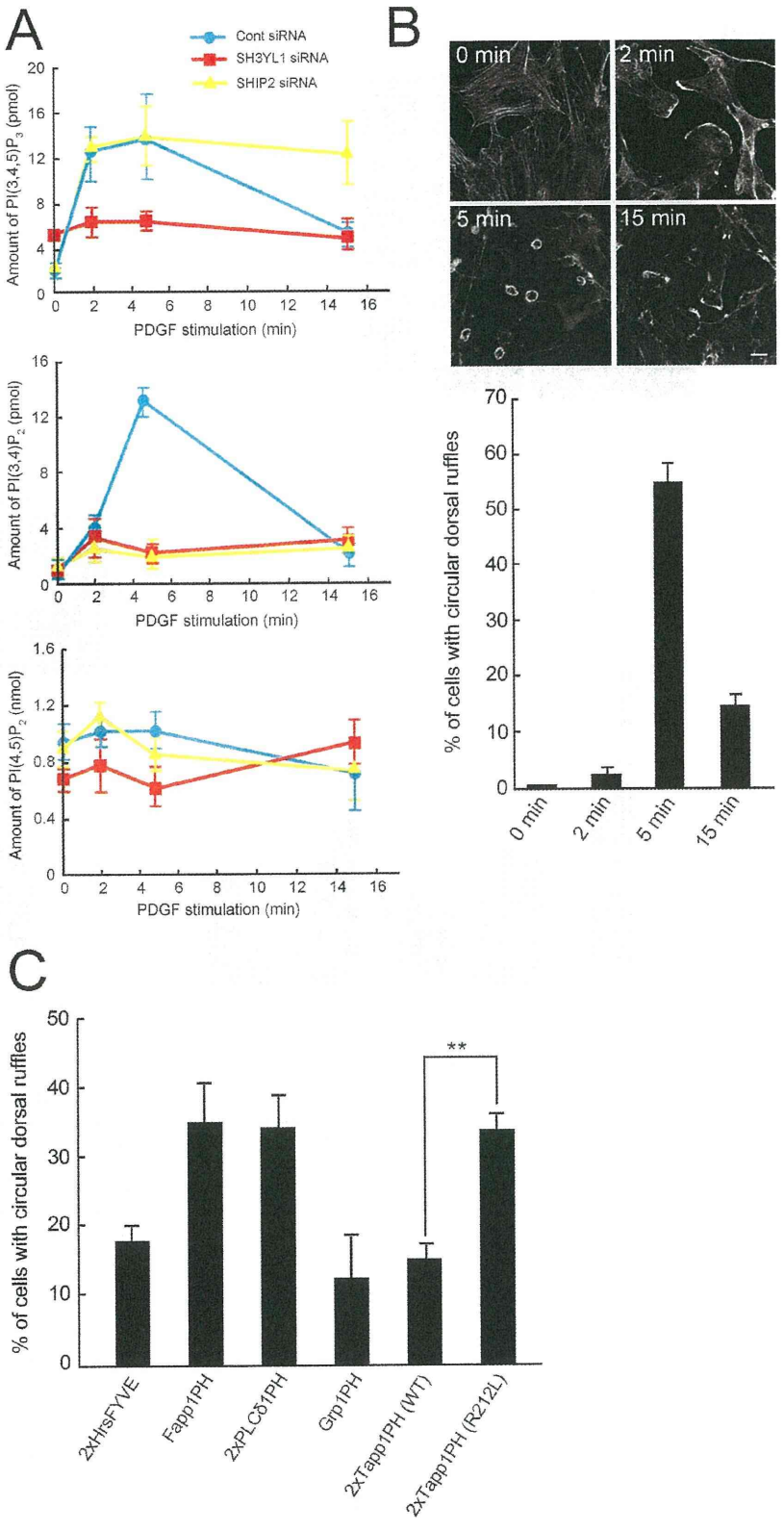

Published May 30, 2011

We noted that overexpression of the Hrs FYVE domain also suppressed dorsal ruffle formation (Fig. 7 C), suggesting that endosomal trafficking is involved.

Dynamics of PI(3,4)P_2 formation and circular dorsal ruffle formation

To examine the molecular dynamics of circular dorsal ruffle formation, the distribution of F-actin, PI(3,4)P_2, SH3YL1, and SHIP2 was monitored in PDGF-stimulated NIH3T3 cells that were transfected with Lifeact-mCherry, a probe for F-actin (Riedl et al., 2008), by time-lapse microscopy. Consistent with the data shown in Fig. 3 A, numerous short F-actin filaments, which appeared to be dorsal ruffle precursors, were observed 3–4 min after stimulation followed by the formation of an F-actin–enriched circular structure at 6 min (Fig. 8 A).

The localization of SH3YL1, SHIP2, and PI(3,4)P_2 was determined in fixed cells. PI(3,4)P_2, which was visualized using Tapp1PH, localized specifically to the mature circular dorsal ruffles at 5 min but was not associated with precursor ruffles at 3 min (Fig. 8 B). In contrast, SH3YL1 and SHIP2 appeared at the precursor structure as early as 3 min, remaining at the mature dorsal ruffles (Fig. 8, B and C). These results suggest that SH3YL1 and SHIP2 are first recruited to the PI(3,4,5)P_3-enriched dorsal ruffle precursors, after which PI(3,4)P_2 is generated and the circular ruffles mature.

Time-lapse microscopy images of NIH3T3 cells expressing Lifeact-mCherry with SH3YL1-GFP or GFP-SHIP2 showed the recruitment of both proteins to the actin-enriched circular structures 3–4 min after PDGF treatment (Fig. S4, A and B). Similarly, PI(3,4,5)P_3 and PI(3,4)P_2 levels rose sequentially at circular dorsal ruffles (Fig. S4 C), indicating that phosphoinositide conversion took place.

Discussion

In this study, we identified the SYLF domain as a novel phosphoinositide-binding module. The SYLF domain also exists in the bacterial genome and is highly conserved in mammals and green plants (Fig. S1 B). The Pfam database and findings from our analysis using the SignalP and LipoP program (Juncker et al., 2003; Emanuelsson et al., 2007) revealed that bacterial proteins harboring the SYLF domain retain putative signal peptides at their N terminus and are thus likely to be exported to the periplasmic space or outer environment. The biochemical and physiological functions of SYLF proteins in the bacteria should be studied to learn about this newly identified lipid-binding module.

Conversely, eukaryotic SYLF domains have the lowest homologies to bacterial members, especially at the ~30 N-terminal residues, but they contain amphipathic α helices. Findings from our in silico and in vitro analyses support that the entire SYLF domain in human SH3YL1, including the amphipathic α helix, is an independent structure (Fig. 1, A and B). Moreover, we have implicated the positively charged residues (Lys14, Lys15, Lys18, and Arg21) in a putative amphipathic α helix in lipid binding (Fig. 2 D). Previous studies have demonstrated that some lipid-binding modules, such as the ENTH and N-terminal amphipathic helix and BAR (N-BAR) domains, have N-terminal amphipathic α helices that mediate membrane curvature generation and/or sensing (Farsad et al., 2001; Ford et al., 2002; Bhatia et al., 2009). With regard to lipid-binding mechanisms, structural analyses of these domains have revealed a single binding pocket in the former and a relatively flat binding surface in the latter, to both of which the N-terminal α helices and the remainder of the region contribute equally (Ford et al., 2002; Gallop et al., 2006). The crystal structure of the SYLF domain will help determine the mechanism by which this novel lipid-binding module recognizes membrane lipids with its amphipathic α helix. We have not observed any curvature dependency in membrane binding by the SYLF domain of SH3YL1 (unpublished data). We are interested in determining whether the SYLF domain retains any membrane-deforming activity, as the ENTH and N-BAR domains have.

Ysc84p/Lsb4p, an SYLF protein in budding yeast, localizes to actin patches at the plasma membrane and binds directly to F-actin through its N-terminal region in vitro (Dewar et al., 2002; Robertson et al., 2009). On the basis of these findings, this region, which corresponds to the SYLF domain in mammals, was termed the Ysc84 actin-binding domain (Robertson et al., 2009). However, despite its significant homology to the Ysc84 actin-binding domain, the SYLF domain of SH3YL1 did not bind to F-actin (Fig. S1 C); instead, it bound to the phosphoinositides, including PI(3,4,5)P_3 (Fig. 1, C and E). The yeast SYLF domains of Ysc84p/Lsb4p and Lsb3p also bound robustly to brain liposomes composed of acidic phospholipids, including PI(4,5)P_2 (Fig. 1 D), indicating that this lipid-binding activity is highly conserved. Because PI(3,4,5)P_3 is believed to be absent in yeast, these SYLF proteins might be used for interactions with phosphoinositides in yeast, such as PI(3,5)P_2 and PI(4,5)P_2.

Using the SH3 domain of SH3YL1 as a probe, we identified several interacting partners, including the PI(3,4,5)P_3 5-phosphatase SHIP2. Our results are consistent with the observation that the SYLF domain binds preferentially to PI(3,4,5)P_3. This model is supported by findings that the SH3 domain deletion mutant (ΔSH3) and the binding-incompetent mutant (W322A) of SH3YL1 were unable to rescue dorsal ruffle formation in the SH3YL1-depleted NIH3T3 cells (Fig. 4 C), suggesting that SHIP2 binding is critical for this process. Similarly, SH3YL1 binding is required for SHIP2 to recover circular dorsal ruffle formation in SHIP2 knockdown cells (Fig. 6 D). On the basis of our results, we propose the following model of dorsal ruffle formation: (a) upon stimulation by growth factors, SH3YL1 is recruited to the dorsal surface of the plasma membrane via interactions between its SYLF domain and PI(3,4,5)P_3; (b) SHIP2 is targeted to the SH3 domain of SH3YL1, where it dephosphorylates PI(3,4,5)P_3, generating PI(3,4)P_2; and (c) Tapp1 is recruited to the PI(3,4)P_2-enriched membrane site, promoting dorsal ruffle formation (Fig. 8 D).

The cellular localization and functions of PI(3,4)P_2 are poorly understood because it has been recognized only as a PI(3,4,5)P_3 metabolite. Recently, our group demonstrated that PI(3,4)P_2 is enriched in and is crucial for the formation of podosomes in Src-transformed NIH3T3 cells (Oikawa et al., 2008).

Published May 30, 2011

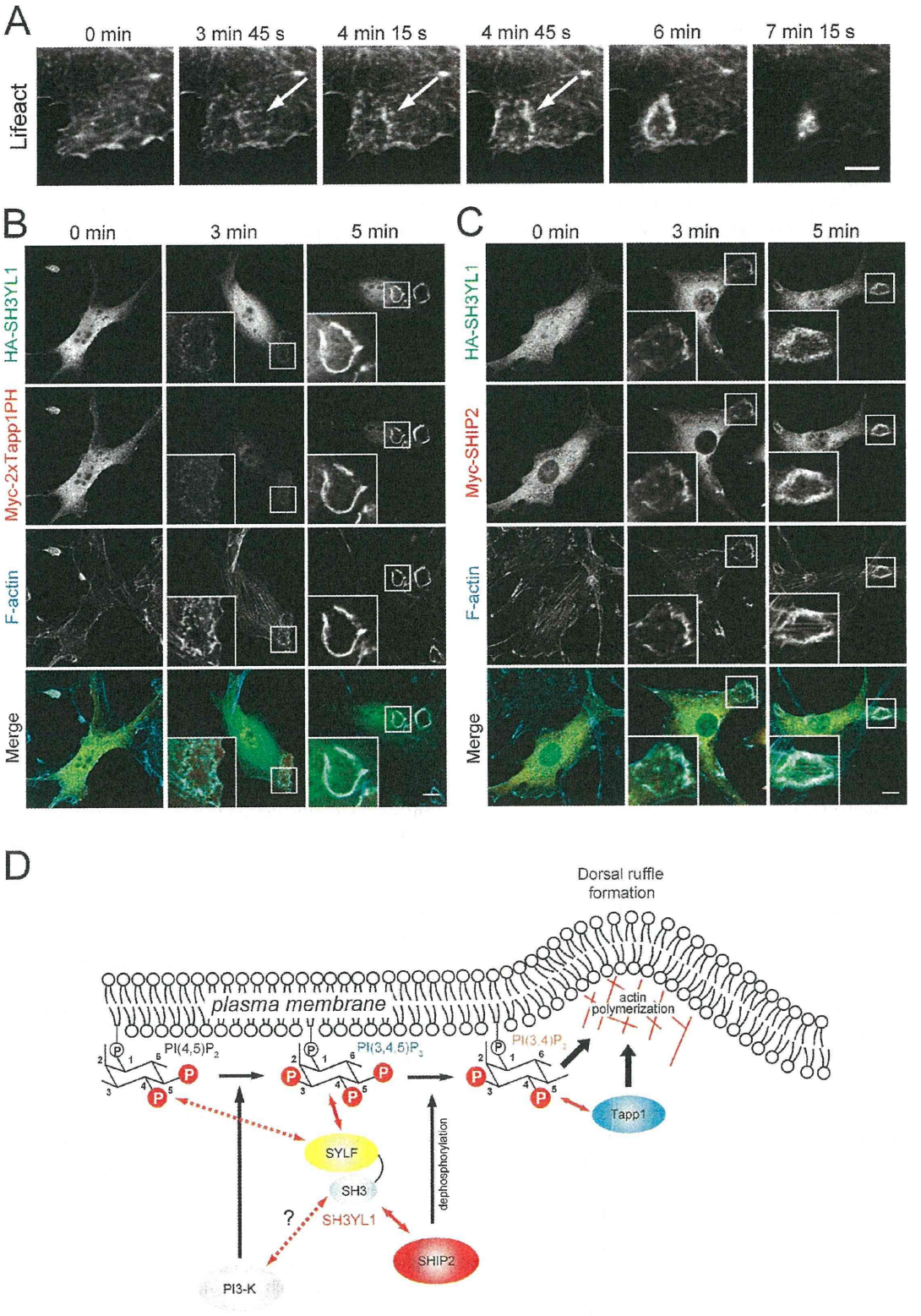

Figure 8. **Dynamics of SH3YL1, SHIP2, and PI(3,4)P_2 at the circular dorsal ruffle.** (A) Time-lapse images of F-actin probed by Lifeact-mCherry transfected in NIH3T3 cells stimulated with 20 ng/ml PDGF. Arrows indicate precursor structures. Bar, 10 µm. (B and C) NIH3T3 cells transiently transfected with HA-SH3YL1 and Myc-2×Tapp1PH (B) or HA-SH3YL1 and Myc-SHIP2 (C) were stimulated with 20 ng/ml PDGF for 3 and 5 min, fixed, and stained with anti-HA, anti-Myc antibodies, and Alexa Fluor 647–phalloidin. Bars, 10 µm. Insets show the boxed areas at high magnification. (D) A model for circular dorsal ruffle formation by SH3YL1 and SHIP2. See Discussion for details.

Published May 30, 2011

The similarity in appearance between the dorsal ruffles and the podosomes, which are circular F-actin–enriched structures, implicates a common mechanism mediated by $PI(3,4)P_2$ and its downstream targets. However, the lipid phosphatases that generate $PI(3,4)P_2$ may differ between these cases, as SHIP2 is essential for dorsal ruffle formation but not for podosomes, which require synaptojanin 2 instead (Oikawa et al., 2008). A recent study has shown that accumulation of $PI(3,4)P_2$ by suppression of INPP4B results in enhanced Akt activation and tumorigenesis (Gewinner et al., 2009). Moreover, INPP4A, another $PI(3,4)P_2$ 4-phosphatase, mediates the suppression of glutamate excitotoxicity in the central nervous system (Sasaki et al., 2010). These studies and the present findings strongly suggest that $PI(3,4)P_2$ is not only a degradation product of $PI(3,4,5)P_3$, but it also has its own functions in vivo.

In addition to SHIP2, SH3YL1 interacted with several proteins such as PI3K-C2β, Tks4, and dynamin 2 through its SH3 domain. We showed that PI3K-C2β is important for the formation of dorsal ruffles (Fig. S3 E). PI3K-C2β phosphorylates phosphatidylinositol to generate PI(3)P in vitro (Sindić et al., 2001; Foster et al., 2003). In support of this, dorsal ruffle formation was blocked by overexpression of Hrs FYVE, which masks PI(3)P on early endosomes. Correspondingly, a recent study has shown that Rab5-mediated endocytosis is required for the activation of Rac on early endosomes to initiate the formation of dorsal circular ruffles (Palamidessi et al., 2008). PI3K-C2α, another isoform of the class II PI3K, alters its substrate specificity when it binds to clathrin in such a manner that facilitates $PI(3,4,5)P_3$ formation (Gaidarov et al., 2001). If this were also the case for PI3K-C2β when it binds to SH3YL1, it would explain the reduction in $PI(3,4,5)P_3$ formation after PDGF stimulation in SH3YL1 knockdown cells (Fig. 7 A). In support of this model, we have observed that $PI(3,4,5)P_3$ production decreases by PI3K-C2β knockdown (Fig. S5 B).

Depletion of Tks4 had minimal effects on dorsal ruffle formation (unpublished data). Tks4 is a scaffolding protein with an N-terminal phox homology domain, four SH3 domains, and several proline-rich motifs, which are required for the formation of the podosome, another circular F-actin structure rich in $PI(3,4)P_2$ (Oikawa et al., 2008; Buschman et al., 2009). Given that podosomes form at the ventral surface of the cell, Tks4 might function with SH3YL1 at the ventral, but not dorsal, side of the plasma membrane.

Dynamin 2 might also contribute to the regulation of the dorsal ruffles in complex with SH3YL1. Previous studies have indicated that dynamin 2 is recruited to the dorsal ruffles, and the expression of a dominant-negative form of dynamin 2 (K44A) strongly inhibits PDGF-induced macropinocytosis (Krueger et al., 2003; Schlunck et al., 2004). Consistent with the findings of a recent study (Liu et al., 2008), the suppression of dynamin 2 by RNAi resulted in the inhibition of dorsal ruffle formation (unpublished data). However, the mechanism underlying SH3YL1 functioning in conjunction with dynamin 2 remains to be determined.

In summary, we have identified a new class of lipid-binding modules, termed the SYLF domain, in SH3YL1. Our data support a model in which the SH3YL1–SHIP2 complex promotes dorsal ruffle formation by conversion of $PI(3,4,5)P_3$ to $PI(3,4)P_2$. Future studies should determine molecular mechanisms by which the downstream targets of these phosphoinositides coordinate the circular array of the actin filaments in the dorsal ruffle.

Materials and methods

Reagents and antibodies

Mouse anti-HA monoclonal antibody and rabbit anti-Myc and anti-SHIP2 polyclonal antibodies were purchased from Cell Signaling Technology. Mouse anti-FLAG monoclonal antibody was purchased from Sigma-Aldrich. Mouse anti–PI3K-C2β monoclonal antibody was obtained from BD, and mouse anti-actin monoclonal antibody was obtained from Millipore. Rabbit anti-Tapp1 and anti-GST polyclonal antibodies were purchased from Santa Cruz Biotechnology, Inc. Anti-SH3YL1 polyclonal antibodies were raised by immunizing rabbits with recombinant SH3YL1 proteins (residues 217–342). All fluorescent reagents (rhodamine, Alexa Fluor 647–phalloidin, and Alexa Fluor 488– and 568–conjugated goat anti–rabbit or anti–mouse secondary antibodies) were purchased from Invitrogen. The bovine brain lipid extract used in the preparation of the brain liposome and phosphatidic acid were purchased from Sigma-Aldrich. Purified phospholipids (phosphatidylinositol, phosphatidylserine, phosphatidylethanolamine [PE], and phosphatidylcholine [PC]) were purchased from Avanti Polar Lipids, Inc. All phosphorylated phosphoinositides (PI(3)P, PI(4)P, PI(5)P, $PI(3,4)P_2$, $PI(3,5)P_2$, $PI(4,5)P_2$, and $PI(3,4,5)P_3$) were obtained from CellSignals Inc. Recombinant human PDGF-BB was obtained from Wako Chemicals USA. LY294002 and trypsin (from bovine pancreas) were purchased from Sigma-Aldrich.

Plasmids

IMAGE clone 3996066 (human SH3YL1) was purchased from Invitrogen, and then the full-length sequence was amplified with specific primers (5′-GCGGATCCATGAATAACCCTATACC-3′ and 5′-GCGTCGACTTAATTCATGGTTACGTAGT-3′) and subcloned into pGEX-6P-1 (GE Healthcare), pEGFP-N3 (Takara Bio Inc.), pCMV-HA, and pEF-BOS-FLAG vectors. SH3YL1 deletion and point mutants were amplified by PCR with specific primers and ligated into each vector. SH3YL1 deletion mutants (ΔSH3 and 1–30) were subcloned into pGEX-6P-3-GFP vector. The yeast Ysc84p (1–218) and Lsb3p (1–218) were amplified from *Saccharomyces cerevisiae* cDNA by PCR with specific primers (5′-GCGGATCCATGGGTATCAATAATCCAAT-3′ and 5′-GCGTCGACAAAGTTGAACGCTCTTGATT-3′ for Ysc84p and 5′-GCGGATCCATGGGTATTAACAATCCTAT-3′ and 5′-GCGTCGACGTAATTAAACGCCCTGGACT-3′ for Lsb3p) and subcloned into pGEX-6P-1 vector. Coding sequences of the human SHIP2 and PI3K-C2β were amplified from HeLa cDNA by PCR with specific primers (5′-GCGAATTCACCATGGCCTCGGCCTGCGGGG-3′ and 5′-GCGTCGACCTTGCTGAGCTGCAGGGTGTCC-3′ for SHIP2 and 5′-GCGAATTCACCATGTCTTCGACTCAGGACA-3′ and 5′-GCGTCGACCAAGGTGCCATGACTTCGAGAT-3′ for PI3K-C2β) and then subcloned into pCMV-Tag3B (Agilent Technologies) and pEGFP-C1 (Takara Bio Inc.) vectors. SHIP2 deletion and point mutants were amplified by PCR with specific primers and ligated into pCMV-Tag3B vector. Human 2×HrsFYVE, Fapp1PH, 2×PLCδ1PH, Grp1PH, 2×Tapp1PH, and 2×Tapp1PH (R212L; lipid-binding inactive form) cDNA fragments were subcloned into pCMV-HA, pCMV-Tag3B, and pTagRFP-C (Evrogen) vectors (Oikawa et al., 2008). Btk-PH-GFP construct was a gift from T. Sasaki (Akita University, Akita, Japan). The mCherry-lifeact construct was generated by Shusaku Kurisu (Kobe University Graduate School of Medicine, Kobe, Japan) as previously described (Riedl et al., 2008). Human Tapp1 cDNA was subcloned into pCMV-HA vector.

Protein expression and purification

Recombinant GST-fusion SH3YL1 (full-length, SYLF, ΔSYLF, and SH3 domain), Ysc84p (1–218), and Lsb3p (1–218) proteins were expressed in BL21 bacterial strain and then purified with glutathione Sepharose 4B (GE Healthcare) according to the manufacturer's instruction. Removal of GST was performed by on-column cleavage with PreScission protease (GE Healthcare). Recombinant FLAG-tagged SH3YL1 (full length and SYLF) and SHIP2 proteins were expressed in FreeStyle 293-F cells (Invitrogen) using FreeStyle MAX reagent (Invitrogen) and then were purified with ANTI-FLAG M2-agarose (Sigma-Aldrich) according to the manufacturer's instruction.

Published May 30, 2011

Proteolytic digestion
1 µg purified FLAG-SH3YL1 (full length and SYLF) proteins was digested in buffer (50 mM Tris, pH 7.5, 10 mM $MgCl_2$, 50 mM KCl, and 1 M urea) with 0.1 µg trypsin for 1, 3, 5, and 10 min at RT. After each reaction was terminated by the addition of 4× sample buffer, the products were analyzed by SDS-PAGE and immunoblotting.

Gel filtration chromatography
Gel filtration chromatography was performed by using a Superdex 75 pg 26/60 column (GE Healthcare) connected with the AKTA prime plus system (GE Healthcare). Protein samples and Gel Filtration Standard (Bio-Rad Laboratories) were loaded onto the column equilibrated with a buffer (50 mM Hepes, pH 7.4, 150 mM NaCl, 1 mM EDTA, and 1 mM DTT).

Cell culture and transfection
HeLa and COS-1 cells were maintained in DME supplemented with 10% FBS, and NIH3T3 cells were maintained in DME supplemented with 10% calf serum. Transfection was performed using Lipofectamine 2000 (Invitrogen) for HeLa and COS-1 cells and using Lipofectamine LTX (Invitrogen) for NIH3T3 cells. Experiments were performed 24 h after transfection.

RNAi
For knockdown of SH3YL1, SHIP2, PI3K-C2β, or Tapp1, validated siRNAs were purchased from Invitrogen. 50 nM siRNAs was transfected into NIH3T3 cells with Lipofectamine RNAiMAX (Invitrogen), and the expression levels were assessed after 72 h by Western blotting or RT-PCR.

Endocytosis assay
To analyze macropinocytosis, cells were starved in serum-free DME for 16 h and then incubated with 1 mg/ml HRP (Invitrogen) in DME ± 20 ng/ml PDGF for 10 min at 37°C. The uptake was stopped by transferring to 4°C, and cells were washed five times with cold PBS with 1 mM $MgCl_2$ and 1 mM $CaCl_2$ and twice with cold PBS. Cells were lysed with PBS containing 0.5% Triton X-100, and aliquots were assayed for enzyme activity (absorbance at 490 nm) by using *O*-phenylenediamine as a substrate and for protein concentration (absorbance at 595 nm) using the BCA Protein Assay kit (Thermo Fisher Scientific). For dextran uptake, cells were starved in serum-free medium for 16 h, incubated with 0.2 mg/ml tetramethylrhodamine-labeled lysine-fixable 10-kD dextran (Invitrogen) in DME ± 20 ng/ml PDGF for 10 min at 37°C, and then were fixed and stained with Hoechst 34580 (Invitrogen) for immunofluorescence.

Immunoblotting and immunoprecipitation
Cells were washed twice with PBS and lysed with lysis buffer (25 mM Hepes, pH 7.5, 0.5% Triton X-100, 2 mM EDTA, and 100 mM NaCl) supplemented with 5 µg/ml aprotinin, 1 µg/ml leupeptin, and 1 mM PMSF. The cell lysates were precleared with immobilized protein A (Thermo Fisher Scientific) and then with FLAG-tagged proteins or SH3YL1 immunoprecipitated with ANTI-FLAG M2-agarose or anti-SH3YL1 antibody for 4 h at 4°C with rotation. Complexes were washed four times in lysis buffer. Immunoprecipitated proteins were analyzed by SDS-PAGE and immunoblotting.

GST pull-down assays
10 mg HeLa cell lysates was mixed with 50 µg GST-SH3 proteins bound to glutathione Sepharose 4B. After incubation for 2 h at 4°C, the beads were washed five times with lysis buffer, and bound proteins were resolved by SDS-PAGE and visualized by Coomassie brilliant blue (CBB). The bands of interest were identified by mass spectrometry.

Immunofluorescence microscopy
Cells were fixed with 3.7% formaldehyde in PBS for 10 min at RT and were then permeabilized with PBS containing 0.2% Triton X-100 for 5 min at RT, washed three times with PBS, and blocked with Image-iT FX signal enhancer (Invitrogen) for 30 min at RT. Cells were incubated with primary antibodies in PBS for 90 min. After three washes with PBS, cells were incubated with the appropriate secondary antibodies in PBS for 1 h. After a brief wash with PBS, coverslips were mounted onto slides using PermaFluor Mountant Medium (Thermo Fisher Scientific) and observed under a FluoView 1000-D confocal microscope (IX81; Olympus) equipped with 473-, 568-, and 633-nm diode lasers (Olympus) through an objective lens (60× oil immersion objective, NA 1.35; Olympus) and with Fluoview software (Olympus). Acquired images were processed with Photoshop (Adobe).

Live cell imaging
NIH3T3 cells transfected with the indicated constructs were grown on glass-base dishes (Iwaki America). Cells were starved in serum-free DME for 16 h and then imaged in the same medium before and after the addition of PDGF (final, 20 ng/ml). The images were acquired for 10–15 min at 15-s intervals by using a FluoView 1000-D confocal microscope through an objective lens (60× oil immersion objective, NA 1.35) at RT.

Liposome cosedimentation assay
Brain lipids (Folch fraction I; Sigma-Aldrich) or mixtures of PE (70%), PC (20%), and 10% of various acidic phospholipids were dried under nitrogen gas and then suspended in 50 µl of buffer (25 mM Hepes, pH 7.5, 100 mM NaCl, and 0.5 mM EDTA) for 1 h at 37°C to allow formation of liposomes. Before mixing with the liposomes, proteins were subjected to centrifugation at 150,000 *g* for 15 min at 4°C to remove aggregated portions. Proteins that came to the supernatant (5 µg) were incubated with the liposomes (25 µg) for 15 min at RT and centrifuged at 150,000 *g* for 20 min at 20°C. Proteins that sedimented with liposomes in the pellet and unbound proteins in the supernatant were separated and then subjected to SDS-PAGE followed by CBB staining.

F-actin binding assay
Rabbit skeletal muscle actin (Cytoskeleton) in G buffer (2 mM Tris, pH 8.0, 0.1 mM $CaCl_2$, 0.2 mM ATP, and 0.5 mM DTT) was first subjected to a centrifugation at 180,000 *g* for 10 min at 4°C. The supernatant (G actin) was incubated in polymerization buffer (2 mM Tris, pH 8.0, 50 mM KCl, 2 mM ATP, and 2 mM $MgCl_2$) for 1 h at RT to form F-actin. Purified recombinant proteins were centrifuged at 180,000 *g* for 10 min at 4°C, and then 5 µg of proteins was incubated with 4 µM F-actin for 30 min at RT and centrifuged at 180,000 *g* for 20 min at 4°C. Proteins in pellet and supernatant were visualized by CBB staining.

Phosphoinositides overlay assay
To label PH domains, pGEX-6P-3-6×Cys was constructed by inserting an oligonucleotide (5′-TGCTGCTGCTGCTGCTGC-3′) into pGEX-6P-3. Each PH domain sequence (Grp1PH, 2×Tapp1PH, and PLCδ1PH) was inserted into this vector, and recombinant proteins were obtained as described in the previous section. The six tandem cysteine residues at the N terminus of each PH domain were labeled with the Qdot (585, 655, and 707) antibody conjugation kit (Invitrogen). Cellular lipids were extracted as previously described (Gray et al., 2003). In brief, cells were scraped with 0.5 M trichloroacetate solution and then incubated with chloroform/methanol (1:2, vol/vol) to remove neutral lipids. The acidic lipids were extracted from the remaining pellets by incubating with chloroform/methanol/HCl (40:80:1, vol/vol/vol). Extracted acidic lipids were dried under nitrogen gas, suspended in chloroform, and then spotted onto nitrocellulose membrane (5 µg each). The membrane was incubated in a blocking buffer (PBS containing 5% skim milk, 1% BSA, and 0.05% Tween 20) for 45 min and then probed with 100 µg/ml Qdot-labeled PH domains in PBS containing 0.05% Tween 20. After 2 h, membranes were washed three times and quantified by a fluorescent image analyzer (FLA-8000; Fujifilm).

RT-PCR
RT-PCR analysis was performed using these primers (5′-GTCACTACCCCTCTCTTCAACTTC-3′ and 5′-GGCTATCCAGGTAGCACTCATACT-3′) for mouse PI3K-C2β cDNA.

Statistical analysis
Statistically significant differences were determined using the Student's *t* test. Differences were considered significant if $P < 0.05$.

Online supplemental material
Fig. S1 shows the evolutionary conservation of SYLF domains and their F-actin binding properties. Fig. S2 shows lipid-binding specificity and dorsal ruffle localization of the SYLF domain–only constructs. Fig. S3 shows that PI3K-C2β and Tapp1 are localized at, as well as required for the formation of, circular dorsal ruffles. Fig. S4 shows the appearances of SH3YL1, SHIP2, $PI(3,4)P_2$, $PI(3,4,5)P_3$, and F-actin at dorsal ruffles revealed by time-lapse microscopy. Fig. S5 shows a dot-blot assay for quantifying phosphoinositide levels after PDGF stimulation. Online supplemental material is available at http://www.jcb.org/cgi/content/full/jcb.201012161/DC1.

We are grateful to Takehiko Sasaki, Shusaku Kurisu, and Yasunori Yamamoto for materials, Naoya Hatano and Yasuhiro Irino for technical assistance, and Hiroyuki Arai, Takao Inoue, Yohko Tanaka-Takiguchi, and Kingo Takiguchi for discussions.

This study was supported in part by a Grant-in-Aid for Creative Scientific Research from the Japan Society for the Promotion of Science (JSPS) to T. Takenawa and T. Itoh, a Grant-in-Aid for Young Scientists from the JSPS to T. Itoh, and Global Centers of Excellence Program grants from the JSPS to J. Hasegawa, H. Hiroaki, T. Takenawa, and T. Itoh.

Published May 30, 2011

Submitted: 27 December 2010
Accepted: 2 May 2011

References

Aoki, N., K. Ito, and M. Ito. 2000. A novel mouse gene, Sh3yl1, is expressed in the anagen hair follicle. *J. Invest. Dermatol.* 114:1050–1056. doi:10.1046/j.1523-1747.2000.00971.x

Araki, N., M.T. Johnson, and J.A. Swanson. 1996. A role for phosphoinositide 3-kinase in the completion of macropinocytosis and phagocytosis by macrophages. *J. Cell Biol.* 135:1249–1260. doi:10.1083/jcb.135.5.1249

Bhatia, V.K., K.L. Madsen, P.Y. Bolinger, A. Kunding, P. Hedegård, U. Gether, and D. Stamou. 2009. Amphipathic motifs in BAR domains are essential for membrane curvature sensing. *EMBO J.* 28:3303–3314. doi:10.1038/emboj.2009.261

Buccione, R., J.D. Orth, and M.A. McNiven. 2004. Foot and mouth: podosomes, invadopodia and circular dorsal ruffles. *Nat. Rev. Mol. Cell Biol.* 5:647–657. doi:10.1038/nrm1436

Buschman, M.D., P.A. Bromann, P. Cejudo-Martin, F. Wen, I. Pass, and S.A. Courtneidge. 2009. The novel adaptor protein Tks4 (SH3PXD2B) is required for functional podosome formation. *Mol. Biol. Cell.* 20:1302–1311. doi:10.1091/mbc.E08-09-0949

Dewar, H., D.T. Warren, F.C. Gardiner, C.G. Gourlay, N. Satish, M.R. Richardson, P.D. Andrews, and K.R. Ayscough. 2002. Novel proteins linking the actin cytoskeleton to the endocytic machinery in *Saccharomyces cerevisiae*. *Mol. Biol. Cell.* 13:3646–3661. doi:10.1091/mbc.E02-05-0262

Dharmawardhane, S., A. Schürmann, M.A. Sells, J. Chernoff, S.L. Schmid, and G.M. Bokoch. 2000. Regulation of macropinocytosis by p21-activated kinase-1. *Mol. Biol. Cell.* 11:3341–3352.

Dowrick, P., P. Kenworthy, B. McCann, and R. Warn. 1993. Circular ruffle formation and closure lead to macropinocytosis in hepatocyte growth factor/scatter factor-treated cells. *Eur. J. Cell Biol.* 61:44–53.

Dyson, J.M., C.J. O'Malley, J. Becanovic, A.D. Munday, M.C. Berndt, I.D. Coghill, H.H. Nandurkar, L.M. Ooms, and C.A. Mitchell. 2001. The SH2-containing inositol polyphosphate 5-phosphatase, SHIP-2, binds filamin and regulates submembraneous actin. *J. Cell Biol.* 155:1065–1079. doi:10.1083/jcb.200104005

Ebina, T., H. Toh, and Y. Kuroda. 2009. Loop-length-dependent SVM prediction of domain linkers for high-throughput structural proteomics. *Biopolymers.* 92:1–8. doi:10.1002/bip.21105

Emanuelsson, O., S. Brunak, G. von Heijne, and H. Nielsen. 2007. Locating proteins in the cell using TargetP, SignalP and related tools. *Nat. Protoc.* 2:953–971. doi:10.1038/nprot.2007.131

Farsad, K., N. Ringstad, K. Takei, S.R. Floyd, K. Rose, and P. De Camilli. 2001. Generation of high curvature membranes mediated by direct endophilin bilayer interactions. *J. Cell Biol.* 155:193–200. doi:10.1083/jcb.200107075

Ford, M.G., I.G. Mills, B.J. Peter, Y. Vallis, G.J. Praefcke, P.R. Evans, and H.T. McMahon. 2002. Curvature of clathrin-coated pits driven by epsin. *Nature.* 419:361–366. doi:10.1038/nature01020

Foster, F.M., C.J. Traer, S.M. Abraham, and M.J. Fry. 2003. The phosphoinositide (PI) 3-kinase family. *J. Cell Sci.* 116:3037–3040. doi:10.1242/jcs.00609

Gaidarov, I., M.E. Smith, J. Domin, and J.H. Keen. 2001. The class II phosphoinositide 3-kinase C2alpha is activated by clathrin and regulates clathrin-mediated membrane trafficking. *Mol. Cell.* 7:443–449. doi:10.1016/S1097-2765(01)00191-5

Gallop, J.L., C.C. Jao, H.M. Kent, P.J. Butler, P.R. Evans, R. Langen, and H.T. McMahon. 2006. Mechanism of endophilin N-BAR domain-mediated membrane curvature. *EMBO J.* 25:2898–2910. doi:10.1038/sj.emboj.7601174

Gewinner, C., Z.C. Wang, A. Richardson, J. Teruya-Feldstein, D. Etemadmoghadam, D. Bowtell, J. Barretina, W.M. Lin, L. Rameh, L. Salmena, et al. 2009. Evidence that inositol polyphosphate 4-phosphatase type II is a tumor suppressor that inhibits PI3K signaling. *Cancer Cell.* 16:115–125. doi:10.1016/j.ccr.2009.06.006

Gray, A., H. Olsson, I.H. Batty, L. Priganica, and C. Peter Downes. 2003. Nonradioactive methods for the assay of phosphoinositide 3-kinases and phosphoinositide phosphatases and selective detection of signaling lipids in cell and tissue extracts. *Anal. Biochem.* 313:234–245. doi:10.1016/S0003-2697(02)00607-3

Heath, R.J., and R.H. Insall. 2008. F-BAR domains: multifunctional regulators of membrane curvature. *J. Cell Sci.* 121:1951–1954. doi:10.1242/jcs.023895

Hogan, A., Y. Yakubchyk, J. Chabot, C. Obagi, E. Daher, K. Maekawa, and S.H. Gee. 2004. The phosphoinositol 3,4-bisphosphate-binding protein TAPP1 interacts with syntrophins and regulates actin cytoskeletal organization. *J. Biol. Chem.* 279:53717–53724. doi:10.1074/jbc.M410654200

Ishihara, H., T. Sasaoka, H. Hori, T. Wada, H. Hirai, T. Haruta, W.J. Langlois, and M. Kobayashi. 1999. Molecular cloning of rat SH2-containing inositol phosphatase 2 (SHIP2) and its role in the regulation of insulin signaling. *Biochem. Biophys. Res. Commun.* 260:265–272. doi:10.1006/bbrc.1999.0888

Itoh, T., and P. De Camilli. 2006. BAR, F-BAR (EFC) and ENTH/ANTH domains in the regulation of membrane-cytosol interfaces and membrane curvature. *Biochim. Biophys. Acta.* 1761:897–912.

Itoh, T., and T. Takenawa. 2002. Phosphoinositide-binding domains: functional units for temporal and spatial regulation of intracellular signalling. *Cell. Signal.* 14:733–743. doi:10.1016/S0898-6568(02)00028-1

Itoh, T., K.S. Erdmann, A. Roux, B. Habermann, H. Werner, and P. De Camilli. 2005. Dynamin and the actin cytoskeleton cooperatively regulate plasma membrane invagination by BAR and F-BAR proteins. *Dev. Cell.* 9:791–804. doi:10.1016/j.devcel.2005.11.005

Juncker, A.S., H. Willenbrock, G. Von Heijne, S. Brunak, H. Nielsen, and A. Krogh. 2003. Prediction of lipoprotein signal peptides in Gram-negative bacteria. *Protein Sci.* 12:1652–1662. doi:10.1110/ps.0303703

Kamioka, Y., S. Fukuhara, H. Sawa, K. Nagashima, M. Masuda, M. Matsuda, and N. Mochizuki. 2004. A novel dynamin-associating molecule, formin-binding protein 17, induces tubular membrane invaginations and participates in endocytosis. *J. Biol. Chem.* 279:40091–40099. doi:10.1074/jbc.M404899200

Kang, H., C. Freund, J.S. Duke-Cohan, A. Musacchio, G. Wagner, and C.E. Rudd. 2000. SH3 domain recognition of a proline-independent tyrosine-based RKxxYxxY motif in immune cell adaptor SKAP55. *EMBO J.* 19:2889–2899. doi:10.1093/emboj/19.12.2889

Krueger, E.W., J.D. Orth, H. Cao, and M.A. McNiven. 2003. A dynamin-cortactin-Arp2/3 complex mediates actin reorganization in growth factor-stimulated cells. *Mol. Biol. Cell.* 14:1085–1096. doi:10.1091/mbc.E02-08-0466

Lanzetti, L., A. Palamidessi, L. Areces, G. Scita, and P.P. Di Fiore. 2004. Rab5 is a signalling GTPase involved in actin remodelling by receptor tyrosine kinases. *Nature.* 429:309–314. doi:10.1038/nature02542

Lee, E., M. Marcucci, L. Daniell, M. Pypaert, O.A. Weisz, G.C. Ochoa, K. Farsad, M.R. Wenk, and P. De Camilli. 2002. Amphiphysin 2 (Bin1) and T-tubule biogenesis in muscle. *Science.* 297:1193–1196. doi:10.1126/science.1071362

Legg, J.A., G. Bompard, J. Dawson, H.L. Morris, N. Andrew, L. Cooper, S.A. Johnston, G. Tramountanis, and L.M. Machesky. 2007. N-WASP involvement in dorsal ruffle formation in mouse embryonic fibroblasts. *Mol. Biol. Cell.* 18:678–687. doi:10.1091/mbc.E06-06-0569

Lemmon, M.A. 2008. Membrane recognition by phospholipid-binding domains. *Nat. Rev. Mol. Cell Biol.* 9:99–111. doi:10.1038/nrm2328

Liu, Y.W., M.C. Surka, T. Schroeter, V. Lukiyanchuk, and S.L. Schmid. 2008. Isoform and splice-variant specific functions of dynamin-2 revealed by analysis of conditional knock-out cells. *Mol. Biol. Cell.* 19:5347–5359. doi:10.1091/mbc.E08-08-0890

Mayer, B.J., and R. Gupta. 1998. Functions of SH2 and SH3 domains. *Curr. Top. Microbiol. Immunol.* 228:1–22.

McMahon, H.T., and J.L. Gallop. 2005. Membrane curvature and mechanisms of dynamic cell membrane remodelling. *Nature.* 438:590–596. doi:10.1038/nature04396

Mellström, K., C.H. Heldin, and B. Westermark. 1988. Induction of circular membrane ruffling on human fibroblasts by platelet-derived growth factor. *Exp. Cell Res.* 177:347–359. doi:10.1016/0014-4827(88)90468-5

Oikawa, T., T. Itoh, and T. Takenawa. 2008. Sequential signals toward podosome formation in NIH-src cells. *J. Cell Biol.* 182:157–169. doi:10.1083/jcb.200801042

Orth, J.D., and M.A. McNiven. 2006. Get off my back! Rapid receptor internalization through circular dorsal ruffles. *Cancer Res.* 66:11094–11096. doi:10.1158/0008-5472.CAN-06-3397

Palamidessi, A., E. Frittoli, M. Garré, M. Faretta, M. Mione, I. Testa, A. Diaspro, L. Lanzetti, G. Scita, and P.P. Di Fiore. 2008. Endocytic trafficking of Rac is required for the spatial restriction of signaling in cell migration. *Cell.* 134:135–147. doi:10.1016/j.cell.2008.05.034

Riedl, J., A.H. Crevenna, K. Kessenbrock, J.H. Yu, D. Neukirchen, M. Bista, F. Bradke, D. Jenne, T.A. Holak, Z. Werb, et al. 2008. Lifeact: a versatile marker to visualize F-actin. *Nat. Methods.* 5:605–607. doi:10.1038/nmeth.1220

Ringstad, N., Y. Nemoto, and P. De Camilli. 1997. The SH3p4/Sh3p8/SH3p13 protein family: binding partners for synaptojanin and dynamin via a Grb2-like Src homology 3 domain. *Proc. Natl. Acad. Sci. USA.* 94:8569–8574. doi:10.1073/pnas.94.16.8569

Robertson, A.S., E.G. Allwood, A.P. Smith, F.C. Gardiner, R. Costa, S.J. Winder, and K.R. Ayscough. 2009. The WASP homologue Las17 activates the

novel actin-regulatory activity of Ysc84 to promote endocytosis in yeast. *Mol. Biol. Cell.* 20:1618–1628. doi:10.1091/mbc.E08-09-0982

Sasaki, J., S. Kofuji, R. Itoh, T. Momiyama, K. Takayama, H. Murakami, S. Chida, Y. Tsuya, S. Takasuga, S. Eguchi, et al. 2010. The PtdIns(3,4)P(2) phosphatase INPP4A is a suppressor of excitotoxic neuronal death. *Nature.* 465:497–501. doi:10.1038/nature09023

Schlunck, G., H. Damke, W.B. Kiosses, N. Rusk, M.H. Symons, C.M. Waterman-Storer, S.L. Schmid, and M.A. Schwartz. 2004. Modulation of Rac localization and function by dynamin. *Mol. Biol. Cell.* 15:256–267. doi:10.1091/mbc.E03-01-0019

Sindić, A., A. Aleksandrova, A.P. Fields, S. Volinia, and H. Banfić. 2001. Presence and activation of nuclear phosphoinositide 3-kinase C2beta during compensatory liver growth. *J. Biol. Chem.* 276:17754–17761. doi:10.1074/jbc.M006533200

Suetsugu, S., D. Yamazaki, S. Kurisu, and T. Takenawa. 2003. Differential roles of WAVE1 and WAVE2 in dorsal and peripheral ruffle formation for fibroblast cell migration. *Dev. Cell.* 5:595–609. doi:10.1016/S1534-5807(03)00297-1

Suyama, M., and O. Ohara. 2003. DomCut: prediction of inter-domain linker regions in amino acid sequences. *Bioinformatics.* 19:673–674. doi:10.1093/bioinformatics/btg031

Swanson, J.A., and C. Watts. 1995. Macropinocytosis. *Trends Cell Biol.* 5:424–428. doi:10.1016/S0962-8924(00)89101-1

Takei, K., V.I. Slepnev, V. Haucke, and P. De Camilli. 1999. Functional partnership between amphiphysin and dynamin in clathrin-mediated endocytosis. *Nat. Cell Biol.* 1:33–39. doi:10.1038/9004

Tsujita, K., S. Suetsugu, N. Sasaki, M. Furutani, T. Oikawa, and T. Takenawa. 2006. Coordination between the actin cytoskeleton and membrane deformation by a novel membrane tubulation domain of PCH proteins is involved in endocytosis. *J. Cell Biol.* 172:269–279. doi:10.1083/jcb.200508091

Warn, R., D. Brown, P. Dowrick, A. Prescott, and A. Warn. 1993. Cytoskeletal changes associated with cell motility. *Symp. Soc. Exp. Biol.* 47:325–338.

Xie, J., I. Vandenbroere, and I. Pirson. 2008. SHIP2 associates with intersectin and recruits it to the plasma membrane in response to EGF. *FEBS Lett.* 582:3011–3017. doi:10.1016/j.febslet.2008.07.048

Yarar, D., C.M. Waterman-Storer, and S.L. Schmid. 2007. SNX9 couples actin assembly to phosphoinositide signals and is required for membrane remodeling during endocytosis. *Dev. Cell.* 13:43–56. doi:10.1016/j.devcel.2007.04.014

Published May 30, 2011

Hasegawa et al., http://www.jcb.org/cgi/content/full/jcb.201012161/DC1

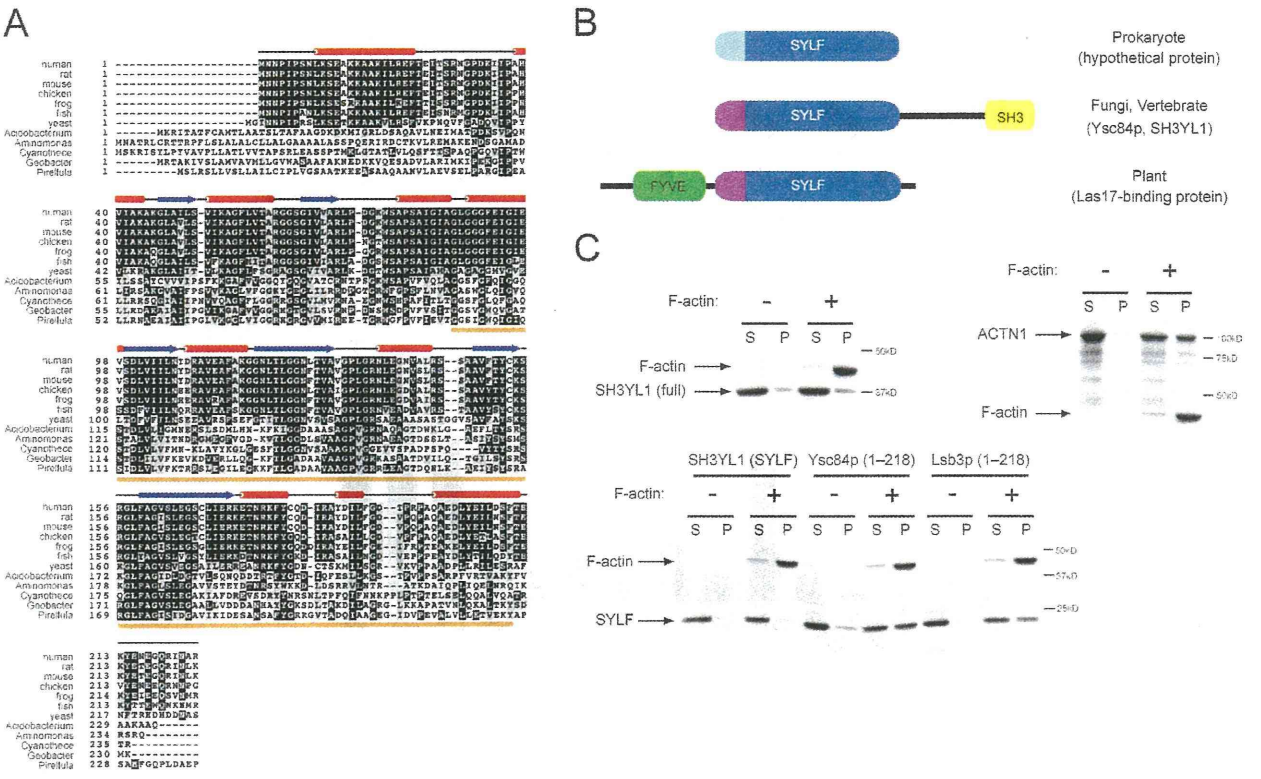

Figure S1. **Multiple sequence alignment of SH3YL1 and F-actin binding assay.** (A) Amino acid sequence alignment of the SYLF domain from bacteria to mammals. The following sequences are aligned (NCBI Protein database accession numbers are given): human (*Homo sapiens*, accession no. AAH08374), rat (*Rattus norvegicus*, accession no. NP_001102175), mouse (*Mus musculus*, accession no. BAA19679), chicken (*Gallus gallus*, accession no. XP_419926), frog (*Xenopus laevis*, accession no. NP_001086532), fish (*Danio rerio*, accession no. XP_694886), budding yeast (*Saccharomyces cerevisiae*, accession no. AAB68945), Acidobacterium (*Terriglobus saanensis*, accession no. YP_004182133), *Aminomonas paucivorans* (accession no. ZP_07740315), *Cyanothece* species (accession no. YP_002484866), *Geobacter* species (accession no. YP_003020897), and *Pirellula staleyi* (accession no. YP_003370784). The columns and arrows show predicted α helices and β strands, respectively. The DUF500 domain defined by the Pfam database is indicated with an orange line. Identical amino acids are shaded in black, and similar residues are in gray. (B) Schematic presentations of SYLF domain–containing proteins. The putative signal peptide is indicated in cyan, and the amphipathic helix is in purple. (C) F-actin and actinin-1, SH3YL1 (full length and SYLF), Ysc84p (1–218), or Lsb3p (1–218) was used in the F-actin binding assay. Proteins in the supernatant (S) and pellet (P) are visualized by CBB staining.

Published May 30, 2011

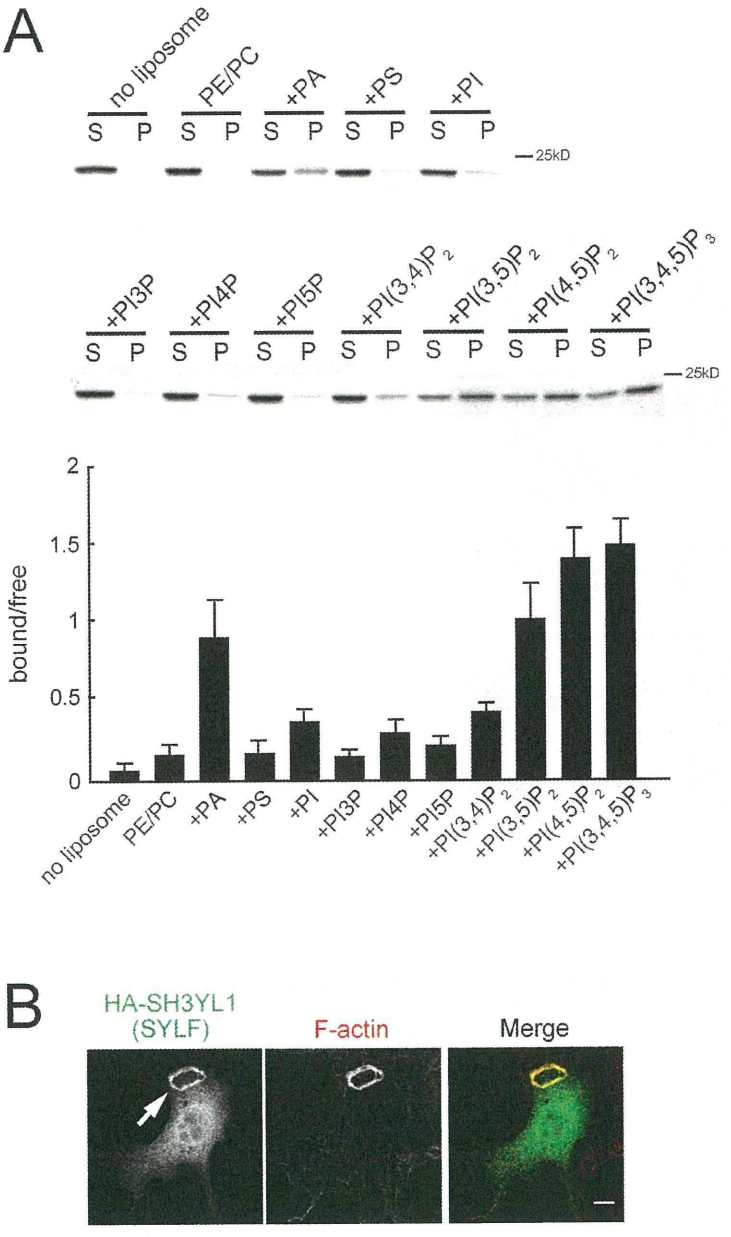

Figure S2. **Lipid specificity of the SYLF domain.** (A) PE/PC-based liposomes supplemented with 10% of the indicated lipids and SH3YL1 (SYLF) were used in the cosedimentation assay and quantitative representation. S, supernatant; P, pellet. Results are a mean (SD) of three independent experiments. (B) NIH3T3 cells transiently transfected with HA-SH3YL1 (SYLF) were serum starved, stimulated with 20 ng/ml PDGF for 5 min, and then fixed and stained with anti-HA antibodies and rhodamine-phalloidin. The arrow indicates the SYLF domain localized to the circular dorsal ruffle. Bar, 10 µm.

Published May 30, 2011

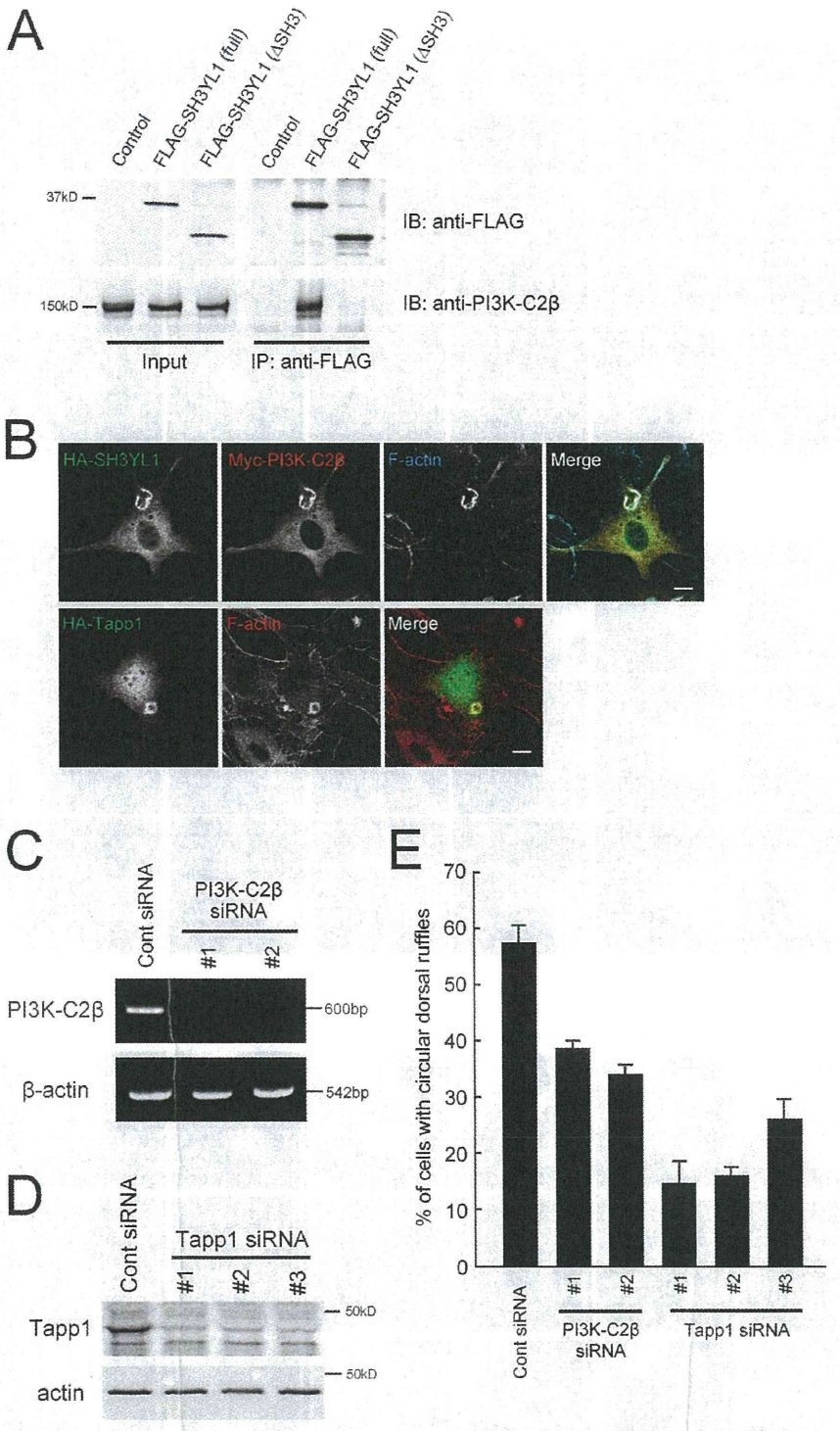

Figure S3. **PI3K-C2β and Tapp1 are required for dorsal ruffle formation.** (A) HeLa cells were transiently transfected with FLAG-SH3YL1 (full length and ΔSH3). Cell lysates were immunoprecipitated (IP) with anti-FLAG antibodies and immunoblotted (IB) with anti-FLAG (top blots) or anti–PI3K-C2β antibodies (bottom blots). (B) NIH3T3 cells expressing HA-SH3YL1 and Myc–PI3K-C2β (top row) or HA-Tapp1 (bottom row) were stimulated with 20 ng/ml PDGF for 5 min and stained with anti-HA, anti-Myc antibodies, and rhodamine- and Alexa Fluor 647–phalloidin. Bars, 10 µm. (C) NIH3T3 cells were transfected for 72 h with siRNA specific to PI3K-C2β or control siRNA. Knockdown levels were assessed by RT-PCR. (D) NIH3T3 cells were transfected for 72 h with siRNA specific to Tapp1 or control siRNA. Knockdown of protein levels is shown by immunoblotting. (E) Percentages of cells treated with control, PI3K-C2β, or Tapp1 siRNAs with at least one circular dorsal ruffle after PDGF stimulation for 5 min. Results are a mean (SD) of three independent experiments; 200 cells counted per experiment.

Published May 30, 2011

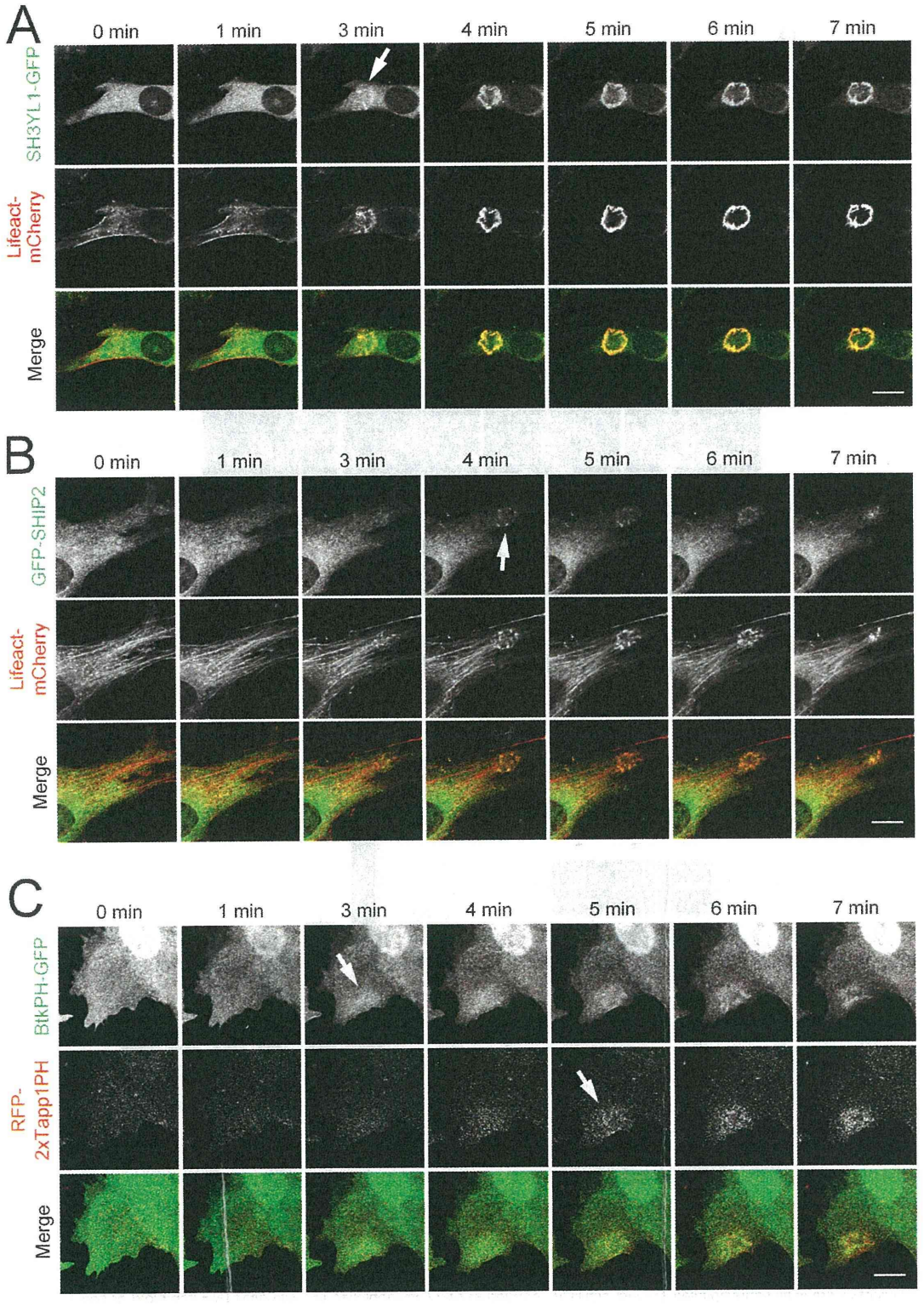

Figure S4. **Live cell imaging during circular dorsal ruffle formation.** NIH3T3 cells transiently transfected with SH3YL1-GFP and Lifeact-mCherry (A), GFP-SHIP2 and Lifeact-mCherry (B), and BtkPH-GFP and TagRFP-2×Tapp1PH (C) were serum starved, and live imaging was performed after adding 20 ng/ml PDGF. Arrows indicate the recruitment of each construct to membrane ruffle structures. Bars, 10 µm.

Published May 30, 2011

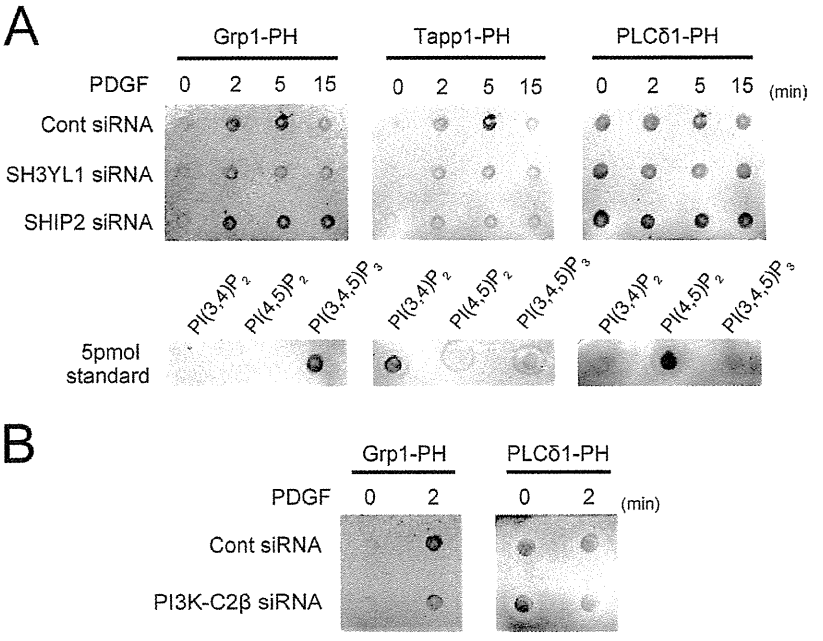

Figure S5. **Phosphoinositide quantification.** (A) NIH3T3 cells treated with SH3YL1, SHIP2, or control siRNA were serum starved and then stimulated with 20 ng/ml PDGF for 0, 2, 5, and 15 min. PI(3,4)P_2, PI(4,5)P_2, and PI(3,4,5)P_3 on nitrocellulose membrane were visualized by dot-blot assay using QD705-Tapp1-2×PH, QD-655-PLCδ1-PH, and QD585-Grp1-PH, respectively. (B) Lipids were extracted from control or PI3K-C2β–depleted NIH3T3 cells stimulated with 20 ng/ml PDGF for 0 and 2 min. PI(3,4,5)P_3 and PI(4,5)P_2 were visualized by dot-blot assay.

Biomol NMR Assign
DOI 10.1007/s12104-011-9317-2

ARTICLE

^{1}H, ^{13}C, and ^{15}N resonance assignment of the SPFH domain of human stomatin

Tomoyuki Tsuruta · Natsuko Goda · Yoshitaka Umetsu · Naoko Iwaya · Yohta Kuwahara · Hidekazu Hiroaki

Received: 20 January 2011 / Accepted: 23 May 2011

Abstract Stomatin, a 288-residue protein, is a component of the membrane skeleton of red blood cells (RBCs), which helps to physically support the membrane and maintains its function. In RBCs, stomatin binds to the glucose transporter GLUT-1 and may regulate its function. Stomatin has a stomatin/prohibitin/flotillin/HflK (SPFH) domain at the center of its polypeptide chain. There are 12 SPFH domain-containing proteins, most of which are localized at the cellular or subcellular membranes. Although the molecular function of the SPFH domain has not yet been established, the domain may be involved in protein oligomerization. The SPFH domain of the archaeal stomatin homolog has been shown to form unique oligomers. Here we report the ^{15}N, ^{13}C, and ^{1}H chemical shift assignments of the SPFH domain of human stomatin [hSTOM(SPFH)]. These may help in determining the structure of hSTOM(SPFH) in solution as well as in clarifying its involvement in protein oligomerization.

Keywords Membrane skeleton · Hereditary stomatocytosis · SPFH domain · Oligomerization

T. Tsuruta · N. Goda · Y. Umetsu · N. Iwaya · Y. Kuwahara · H. Hiroaki (✉)
Division of Structural Biology, Graduate School of Medicine, Kobe University, 7-5-1, Kusunoki-cho, Chuo-ku, Kobe, Hyogo 650-0017, Japan
e-mail: hiroakih@med.kobe-u.ac.jp

N. Goda · Y. Umetsu · H. Hiroaki
The Structural Biology Research Center and Division of Biological Sciences, Graduate School of Science, Nagoya University, Furo-cho, Chikusa-ku, Nagoya 464-8601, Japan

N. Iwaya
Department of Molecular Engineering, Graduate School of Engineering, Kyoto University, Kyoto 615-8510, Japan

Y. Kuwahara
Life BEANS (Bio Electromechanical Autonomous Nano Systems) Center, BEANS Project, Hachioji, Tokyo 192-0982, Japan

H. Hiroaki
Global-COE (Center of Excellence) Program for Integrative Membrane Biology, Kobe University, Kobe, Japan

Biological context

Stomatin, a band 7.2 protein, is a major component of the membrane skeleton in red blood cells (RBCs) (Green et al. 2004). It is also expressed in many vertebrate tissues and cell lines (Green et al. 2004). Stomatin homologs are evolutionarily conserved in eukaryotes as well as in bacteria and archaea. An inherited anemia, called stomatocytosis, is characterized by "leaky" RBCs in which stomatin is completely absent (Green et al. 2004). Stomatin is believed to maintain membrane structure, thereby reducing the leakage of monovalent cations from RBCs. It regulates the gating of acid-sensing ion channels, which are non-voltage-gated Na^{+} channels found in mammalian neurons (Price et al. 2004). Stomatin also binds to the glucose transporter GLUT-1 and regulates its activity (Zhang et al. 1999). However, the molecular function of stomatin is not fully understood.

Stomatin has a transmembrane region at the N-terminus and a stomatin/prohibitin/flotillin/HflK/C (SPFH) domain, followed by a coiled-coil region. The SPFH domain of human stomatin [residues 94–202, hSTOM(SPFH)] shows striking sequence conservation of greater than 96% among all mammals. The corresponding sequences of African clawed frog and zebrafish still share 94 and 91% sequence identity, respectively, suggesting the physiological

Published online: 05 June 2011

importance of the region. However, a common biological function for the SPFH domain has not been established.

In the human genome, there are 12 SPFH domain-containing proteins, which include flotillin, prohibitin, podocin, and stomatin-like proteins. In many cases, SPFH proteins form oligomers using their C-terminal coiled-coil region (Langhorst et al. 2005). In addition, we recently reported that the SPFH domain from *Pyrococcus horikoshii* PH0470 forms various oligomers and a polymer even without the coiled-coil region C-terminal to the domain (Kuwahara et al. 2009). Based on an NMR study of the metastable PH0470(SPFH) domain dimer and trimer, we reported the 3D domain swap model (Kuwahara et al. 2009). It should be noted that the backbone fold of the SPFH domain adopts a two-layer structure of an α-helical sub domain and a β-sheet sub domain connected by two linker regions at one side of the domain, which allows it to form 3D-domain swapped oligomers.

In this study, we moved on to hSTOM(SPFH) of human RBCs from archaeal stomatin. We hypothesized that this stomatin may form oligomers through a 3D domain-swapping mechanism on the SPFH domain as well as its coiled-coil region. To assess this hypothesis, the complete assignment of the NMR signals of the hSTOM(SPFH) domain as well as the determination of its structure in solution are good starting points.

Methods and experiments

Sample preparation

The domain boundary of the SPFH domain of human stomatin was carefully designed from the multiple sequence alignment between mammalian stomatins and archaeal stomatin homologs including PH0470 (Kuwahara et al. 2009) and PH1511. The expression vector for the recombinant GST fusion proteins of hSTOM(SPFH) (residues 94–202) was constructed using the PRESAT-vector methodology, derived from the pGEX-4T3 vector (GE Healthcare) (Goda et al. 2004). An isotopically labeled protein for NMR spectroscopy was generated in *Escherichia coli* BL21(*DE3*) from 1 L M9 minimal medium culture grown at 30°C in the presence of [^{15}N]-NH_4Cl and [^{13}C] glucose as the sole nitrogen and carbon sources, respectively. The harvested cells were resuspended in the lysis buffer (50 mM Tris–HCl, pH 7.5, 150 mM NaCl) and disrupted by sonication. The cell lysate was cleared by centrifugation and then applied to a DEAE-Sepharose column (GE Healthcare). It was further purified by glutathione-Sepharose affinity chromatography (GE Healthcare).

The GST tag was removed by thrombin "on-beads," and the protease was removed using benzamidine-Sepharose (GE Healthcare). Next, the SPFH domain was purified by gel filtration using a HiLoad 26/60 Superdex 75 pg column (GE Healthcare). Using this purification protocol, ^{15}N-labeled or ^{13}C,^{15}N-doubly–labeled protein was prepared. A typical yield of the labeled hSTOM(SPFH) was 9.7 mg from 1 L M9 culture. The purified protein was concentrated to 0.6 mM and dialyzed with 50 mM sodium phosphate (pH 6.4) and 100 mM NaCl.

NMR spectroscopy

NMR experiments were performed on a Bruker *Avance* III (600 MHz) NMR spectrometer (Bruker), which was equipped with a cryogenic triple-resonance probe. For the assignment of the backbone ^{1}H, ^{13}C, and ^{15}N resonances, HNCA, HN(CO)CA, HNCACB, CBCA(CO)NH, HNCO, HN(CA)CO, and 3D ^{15}N-edited NOESY-HSQC spectra were recorded (Cavanagh et al. 2006). For the side-chain resonance assignment, 2D constant-time ^{1}H-^{13}C HSQC, 3D ^{13}C-edited NOESY-HSQC, HCCH-TOCSY, CC(CO)NNH, and HCC(CO)NNH spectra were recorded. All NMR spectra were recorded at 298 K. All spectra were processed using NMRPipe (Delaglio et al. 1995) and analyzed using the SPARKY (Goddard and Kneller 2004).

Assignments and data deposition

The HSQC spectra of hSTOM(SPFH) showed a good dispersion of all backbone amide signals (Fig. 1). The sequential assignment of backbone signals was initiated by the automated program MARS (Jung and Zweckstetter 2004), resulting in approximately 65% completion. Subsequent iterative MARS runs further increased the assignment gains up to 80%. We then carefully traced the sequential connectivities based on triple-resonance data sets with the help of the ^{15}N-edited NOESY spectra. Following a sequential assignment procedure, 99.1% of the $^{1}H^{N}$, ^{15}N resonances of the backbone amide groups (108 out of 109 non-Pro residues) were assigned (Fig. 1). In addition, 96.5% of H^{α} (109 out of 113 residues), 96.5% of $^{13}C^{\alpha}$ (109 out of 113 residues), and 98.2% of $^{13}C^{\beta}$ (107 out of 109 residues) resonances were assigned. Finally, 86.3% of all ^{1}H, ^{13}C, and ^{15}N resonances (1,338 out of 1,551 atoms, including side-chain atoms) were assigned. Unassigned atoms mainly included side-chain atoms which cannot be assigned using standard protein NMR protocol, e.g. Tyr Cγ, Cζ, Asn Cγ, and Gln Cδ. We also provided the ^{13}C secondary chemical shifts and the secondary structure of hSTOM(SPFH) (Fig. 2). This result indicates that

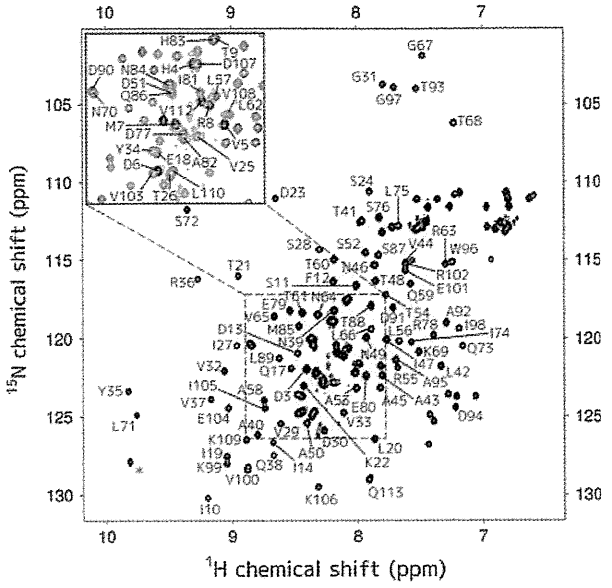

Fig. 1 A portion of the ^{15}N-^{1}H-HSQC spectrum of the SPFH domain of human stomatin illustrating a number of assigned backbone ^{15}N resonances. *Asterisk* indicates the Trp96 side chain

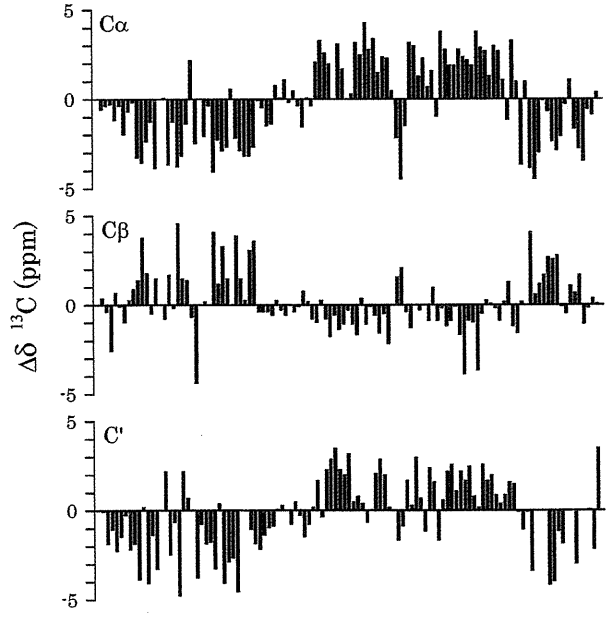

Fig. 2 Secondary chemical shifts of the SPFH domain of human stomatin for Cα, Cβ, and C′ from CSI consensus value

hSTOM(SPFH) is a α/β-fold domain composed of three regions, β1 region (residues 5–36), α region (residues 50–92), and β2 region (residues 98–109), as well as other SPFH domains.

Because it was prepared from the GST-fusion protein construct, the NMR sample must contain the four extra residues (GSDH) preceding the N-terminus in human stomatin (residues 94–202). Thus, in the chemical shift data deposited at the BioMagResBank and Fig. 1, the residues 1–4 correspond to GSDH from the expression vector, whereas the residues 5–113 are equivalent to the residues 94–202 of full-length human stomatin. The resonance assignments obtained in this study were useful to determine the structure of hSTOM(SPFH) in solution. The data may also give some insight into its involvement in stomatin self-oligomerization. All available ^{1}H, ^{13}C, and ^{15}N chemical shifts of backbone and side-chain resonances of hSTOM(SPFH) have been deposited in the BioMagResBank under accession number 11425.

Acknowledgments This work was supported by Takeda Science Foundation and Suzuken Memorial Foundation. The authors are grateful to Mr. R. Taniguchi for his help in preparing the figure.

References

Cavanagh J, Fairbrother WJ, Palmer AGIII, Rance M, Skelton NJ (2006) Protein NMR spectroscopy, 2nd edn. Academic Press, San Diego, pp 533–678, 781–817

Delaglio F, Grzesiek S, Vuister GW, Zhu G, Pfeifer J, Bax A (1995) NMR Pipe: a multidimensional spectral processing system based on UNIX pipes. J Biomol NMR 6:277–293

Goda N, Tenno T, Takasu H, Hiroaki H, Shirakawa M (2004) The PRESAT-vector: asymmetric T-vector for high-throughput screening of soluble protein domains for structural proteomics. Protein Sci 13:652–658

Goddard TD, Kneller DG (2004) Sparky 3. University of California, San Francisco

Green JB, Fricke B, Chetty MC, von During M, Preston GF, Stewart GW (2004) Eukaryotic and prokaryotic stomatins: the proteolytic link. Blood Cells Mol Dis 32:411–422

Jung YS, Zweckstetter M (2004) Mars–robust automatic backbone assignment of proteins. J Biomol NMR 30:11–23

Kuwahara Y, Unzai S, Nagata T, Hiroaki Y, Yokoyama H, Matsui I, Ikegami T, Fujiyoshi Y, Hiroaki H (2009) Unusual thermal disassembly of the SPFH domain oligomer from *Pyrococcus horikoshii*. Biophys J 97:2034–2043

Langhorst MF, Reuter A, Stuermer CA (2005) Scaffolding microdomains and beyond: the function of reggie/flotillin proteins. Cell Mol Life Sci 62:2228–2240

Price MP, Thompson RJ, Eshcol JO, Wemmie JA, Benson CJ (2004) Stomatin modulates gating of acid-sensing ion channels. J Biol Chem 279:53886–53891

Zhang JZ, Hayashi H, Ebina Y, Prohaska R, Ismail-Beigi F (1999) Association of stomatin (band 7.2b) with Glut1 glucose transporter. Arch Biochem Biophys 372:173–178

THE JOURNAL OF BIOLOGICAL CHEMISTRY VOL. 286, NO. 24, pp. 21732–21741, June 17, 2011

Structure and Function of the N-terminal Nucleolin Binding Domain of Nuclear Valosin-containing Protein-like 2 (NVL2) Harboring a Nucleolar Localization Signal*[S]

Received for publication, August 12, 2010, and in revised form, February 28, 2011 Published, JBC Papers in Press, April 7, 2011, DOI 10.1074/jbc.M110.174680

Yoshie Fujiwara[‡§¶], Ken-ichiro Fujiwara[‖], Natsuko Goda[‡¶], Naoko Iwaya[‡¶‡‡], Takeshi Tenno[‡§], Masahiro Shirakawa[‡‡], and Hidekazu Hiroaki[‡§¶1]**

*From the [‡]Division of Structural Biology, Graduate School of Medicine, and the [§]Global Center of Excellence Program for Integrative Membrane Biology, Kobe University, 7-5-1 Kusunokicho, Chuo-ku, Kobe, Hyogo 650-0017, Japan, the [¶]Institute for Bioinformatics Research and Development, Japan Science and Technology Agency, Kawaguchi Center Building, 4-1-8, Honcho, Kawaguchi, Saitama 332-0012, Japan, the [‖]Field of Supramolecular Biology, International Graduate School of Arts and Sciences, Yokohama City University, 1-7-29 Suehirocho, Tsurumi-ku, Yokohama, Kanagawa 230-0045, Japan, **Shionogi Research Laboratories, Shionogi & Co., Ltd., 5-12-4 Sagisu, Fukushima-ku, Osaka 553-0002, Japan, and the [‡‡]Department of Molecular Engineering, Graduate School of Engineering, Kyoto University, Kyoto-daigaku Katsura, Nishikyo-ku, Kyoto 615-8510, Japan*

The N-terminal regions of AAA-ATPases (ATPase associated with various cellular activities) often contain a domain that defines the distinct functions of the enzymes, such as substrate specificity and subcellular localization. As described herein, we have determined the solution structure of an N-terminal unique domain isolated from nuclear valosin-containing protein (VCP)-like protein 2 ($NVL2^{UD}$). $NVL2^{UD}$ contains three α helices with an organization resembling that of a winged helix motif, whereas a pair of β-strands is missing. The structure is unique and distinct from those of other known type II AAA-ATPases, such as VCP. Consequently, we identified nucleolin from a HeLa cell extract as a binding partner of this domain. Nucleolin contains a long (~300 amino acids) intrinsically unstructured region, followed by the four tandem RNA recognition motifs and the C-terminal glycine/arginine-rich domain. Binding analyses revealed that $NVL2^{UD}$ potentially binds to any of the combinations of two successive RNA binding domains in the presence of RNA. Furthermore, $NVL2^{UD}$ has a characteristic loop, in which the key basic residues RRKR are exposed to the solvent at the edge of the molecule. The mutation study showed that these residues are necessary and sufficient for nucleolin-RNA complex binding as well as nucleolar localization. Based on the observations presented above, we propose that NVL2 serves as an unfoldase for the nucleolin-RNA complex. As inferred from its RNA dependence and its ATPase activity, NVL2 might facilitate the dissociation and recycling of nucleolin, thereby promoting efficient ribosome biogenesis.

Nuclear valosin-containing protein (VCP)[2]-like protein (NVL) was first identified as a gene product that displays a high level of amino acid similarity with an AAA-ATPase, VCP/p97. AAA-ATPases, associated with various cellular activities, are hexameric ATP-hydrolyzing enzymes found in all three kingdoms of life. They play important roles in various cellular processes, including the dissociation of protein complexes and protein translocation (1–4). The AAA-ATPases are characterized by the presence of one (type I) or two (type II) copies of a well conserved catalytic ATPase domain comprising 220–250 amino acids. NVL is classified as a type II AAA-ATPase with two tandem AAA domains. In fact, NVL has two alternatively spliced isoforms, a short form, NVL1, and a long form, NVL2, which are produced from different methionines as the translation initiation sites (Fig. 1) (5). NVL2 resides in the nucleolus, where it is involved in the biogenesis of the 60 S ribosomal subunit. In this pathway, the ribosomal subunit RPL5 and the DNA helicase DOB1 have been identified as NVL2-binding proteins (6, 7). Other well known NVL orthologs include *small-minded* (*smid*), a *Drosophila* ortholog (7, 8); a CED-4-interacting protein, Mac-1, a *Caenorhabditis elegans* ortholog (9); and a more distant *Saccharomyces cerevisiae* homolog, Rix7p (10, 11). The cellular roles of these nonvertebrate NVL orthologs are only partially consistent with each other. Consequently, further analysis of this molecule from a structural viewpoint is needed.

Despite the sequence similarity between VCP/p97 and NVL in their AAA regions, the N-terminal regions of NVL2 ($NVL2^{UD}$) and VCP/p97 are different. The two proteins reside in different subcellular locations; VCP/p97 is in the cytoplasm, nucleus, and endoplasmic reticulum membrane, whereas NVL is exclusively localized in the nucleolus (5, 6). The amino acid sequences of the N-terminal regions are variable, in contrast to the high sequence conservation of the AAA domains. The

* This study was supported in part by the Japan Science and Technology Agency Institute for Bioinformatics Research and Development and by a grant-in-aid for scientific research on Innovative Areas. This work was also supported by Grant-in-aid for Scientific Research (c) 22570118 from the Japanese Ministry of Education, Culture, Sports, Science, and Technology (to H. H.).

[S] The on-line version of this article (available at http://www.jbc.org) contains supplemental Tables S1–S3 and Figs. S1–S4.

The atomic coordinates and structure factors (code 2rre) have been deposited in the Protein Data Bank, Research Collaboratory for Structural Bioinformatics, Rutgers University, New Brunswick, NJ (http://www.rcsb.org/).

The chemical shift assignments have been deposited in the BioMagResBank, under the accession code 11250 (http://www.bmrb.wisc.edu).

[1] To whom correspondence should be addressed. Tel.: 81-78-382-5813; Fax: 81-78-382-5816; E-mail: hiroakih@med.kobe-u.ac.jp.

[2] The abbreviations used are: VCP, valosin-containing protein; AAA, ATPases associated with various cellular activities; NVL, nuclear VCP-like protein; $NVL2^{UD}$, nuclear VCP-like protein 2 unique domain; NoLS, nucleolar localization signal; NTD, N-terminal domain; NSF, *N*-ethylmaleimide-sensitive fusion protein; NLS, nuclear localization signal; RRM, RNA recognition motif; GAR, glycine/arginine-rich; PDB, Protein Data Bank.